Unravelling megaturbidite deposition: Evidence for turbidite stacking/amalgamation and seiche influence during the 1601 CE earthquake at Lake Lucerne, Switzerland

FLOR VERMASSEN*·† , MAARTEN VAN DAELE† , NORE PRAET†·‡ ,
VEERLE CNUDDE§·¶ , CATHERINE KISSEL** and FLAVIO S. ANSELMETTI††
*Department of Geological Sciences, Stockholm University, Stockholm, Sweden
(E-mail: flor.vermassen@geo.su.se)
†Renard Centre of Marine Geology, Department of Geology, Ghent University, Ghent, Belgium
‡Flanders Marine Institute (VLIZ), InnovOcean Campus, Ostend, Belgium
§Centre of X-ray Tomography-PProGRess, Department of Geology, Ghent University, Ghent, Belgium
¶Department of Earth Sciences, Utrecht University, Utrecht, The Netherlands
**Laboratoire des Sciences du Climat et de l'Environnement/IPSL, CEA-CNRS-UVSQ, Université Paris-
Saclay, Gif-sur-Yvette, France
††Institute of Geological Sciences and Oeschger Centre for Climate Change Research, University of
Bern, Bern, Switzerland

ABSTRACT

Megaturbidites are commonly used to reconstruct the seismic history (palaeo-seismology) of areas where large earthquakes occur. However, the depositional mechanisms and sedimentary characteristics of these deposits are not yet fully understood. This study unravels the sequence of sediment deposition that occurred in Lake Lucerne (Vitznau Basin) following the 1601 CE earthquake in central Switzerland. During this event, slope failures were triggered, generating mass flows and turbidity currents that led to the formation of mass-transport deposits and a megaturbidite. These deposits are sampled in 28 sediment cores, which are examined with X-ray computed tomography scans (medical and μCT), grain-size analysis and natural remanent magnetisation. This suite of analyses allows a detailed reconstruction of turbidite stacking and amalgamation in the centre of the basin, followed by settling of finer sediments influenced by a lake seiche. Initial deposition of mass-transport deposits is followed by sandy turbidites reaching the depocentre. Some of these turbidite sands can be linked to their source areas, and evidence is found of some turbidites being overridden by mass flows in the peripheral parts of the megaturbidite deposit. Hereafter, sedimentation becomes controlled by seiche-induced currents, which rework fine sediments upon deposition, leading to subtle grain-size variations at the base of the seiche-influenced sub-unit and a ponded geometry of the megaturbidite. As the seiche movement dampens, a relatively muddy, homogeneous sub-unit is deposited that drapes the basin plain. Overall, this study provides the first highly detailed sedimentological analysis of megaturbidite deposition in a lake, demonstrating the distinct sedimentological imprint of lake seiching and turbidite amalgamation/stacking. This will improve the recognition and interpretation of earthquake-induced megaturbidites in other lake records or isolated basins, and demonstrates the value of using (μ)CT scans in combination with traditional sedimentological parameters to reconstruct the depositional processes of megaturbidites.

INTRODUCTION

To better understand the history of large earthquakes trough time, deposits known as megaturbidites are often used to reconstruct earthquake recurrence in areas where lake or ocean basins offer sedimentary sinks (e.g. Schnellmann *et al.*, 2006; Fanetti *et al.*, 2008; Leithold *et al.*, 2019; Praet *et al.*, 2022). The term 'megaturbidite' refers to thick, extensive, relatively homogenous sediments deposited by a turbidity current (Bouma, 1987). While megaturbidites are commonly associated with earthquake shaking, they can also be triggered in the absence of seismic activity (Reeder *et al.*, 2000; Zuffa *et al.*, 2000; Girardclos *et al.*, 2007). Therefore, there is a strong need to identify sedimentary features that can be used to discriminate seismic from non-seismic megaturbidites. The widely accepted 'synchronicity criterion' proposes that multiple, synchronous slope failures are indicative of earthquake shaking (Kastens, 1984; Adams, 1990; Schnellmann *et al.*, 2006). Such synchronous slope failures can be evidenced in the basins by amalgamated turbidites, because these are formed by the simultaneous deposition from several turbidity currents that arrive from a single or multiple directions, evidenced by coarse-grained 'pulses' or repetitions of Bouma sequence divisions (Nakajima & Kanai, 2000; Gutiérrez-Pastor *et al.*, 2013; Polonia *et al.*, 2013; Van Daele *et al.*, 2014, 2017).

Unravelling the depositional processes in lakes or oceans during and following earthquakes is complex because deposition of (mega)turbidites may be affected by additional phenomena, such as tsunamis or seiching. A seiche is a standing wave in a (semi-)enclosed basin that results in an oscillatory movement of the water level. A so-called seismic seiche typically occurs when the basin's natural period is similar to that of the seismic waves (Kvale, 1955) and has been observed in pools (Avşar *et al.*, 2014), fjords (Kvale, 1955; Bondevik *et al.*, 2013) and lakes (Kvale, 1955; Granin *et al.*, 2018). However, lake seiches can also be triggered by tectonic tilting of the lake (McCulloch, 1966), or by large-scale, basin-wide landslides, which has for example been observed in Lake Lucerne after the 1601 CE earthquake (Siegenthaler *et al.*, 1987).

Reworking and deposition of lake sediment by seiche waves has been interpreted to be the dominant sedimentation process during earthquake shaking by some authors (Siegenthaler *et al.*, 1987; Chapron *et al.*, 1999). These event deposits consist of a muddy, thick homogeneous bed with sandy to silty laminae at their base, referred to as 'homogenites' (Kastens & Cita, 1981; Cita *et al.*, 1996; Chapron *et al.*, 1999; Bertrand *et al.*, 2008), but have the same characteristics as megaturbidites (Mulder *et al.*, 2009), although the sandy base is sometimes referred to as 'turbidite' and separated from the 'homogenite' (Carrillo *et al.*, 2008; Çağatay *et al.*, 2012; Campos *et al.*, 2013). Such seiche-influenced deposits in the deepest part of the basin typically have a basin-focused geometry that results from gradual deposition by a sediment cloud, suspended by seiche currents (Siegenthaler *et al.*, 1987; Chapron *et al.*, 1999; Beck, 2009; Mulder *et al.*, 2009; Van Daele *et al.*, 2015). The coarse-grained laminae at the base of these event deposits are interpreted as the result of reworking by seiche-wave induced bottom currents, while finer sediments settle from suspension when the bottom currents cease (Siegenthaler *et al.*, 1987; Chapron *et al.*, 1999; Beck, 2009; Hilbe & Anselmetti, 2014). Hence, both synchronous slope failures (turbidite amalgamation) and seiching have been proposed to lead to grain-size fluctuations near the base of a megaturbidite, but distinguishing one from the other is challenging. Since high-quality palaeoseismic reconstructions rely on a confident recognition of earthquake-related deposits, it is key to understand the depositional processes involved. In part, the understanding of the depositional process of megaturbidites has been hampered because their interpretation is often based on the analysis of a single or limited number of cores (e.g., Schnellmann *et al.*, 2006; Campos *et al.*, 2013; Van Daele *et al.*, 2015).

This study uses an array of sediment cores to investigate a well-known megaturbidite in Lake Lucerne (Vitznau Basin), triggered by the 1601 CE central Switzerland earthquake. While it has been shown that this megaturbidite is the result of multiple synchronously triggered slope failures forming the Weggis slide complex (Fig. 1; Schnellmann *et al.*, 2002), turbidite
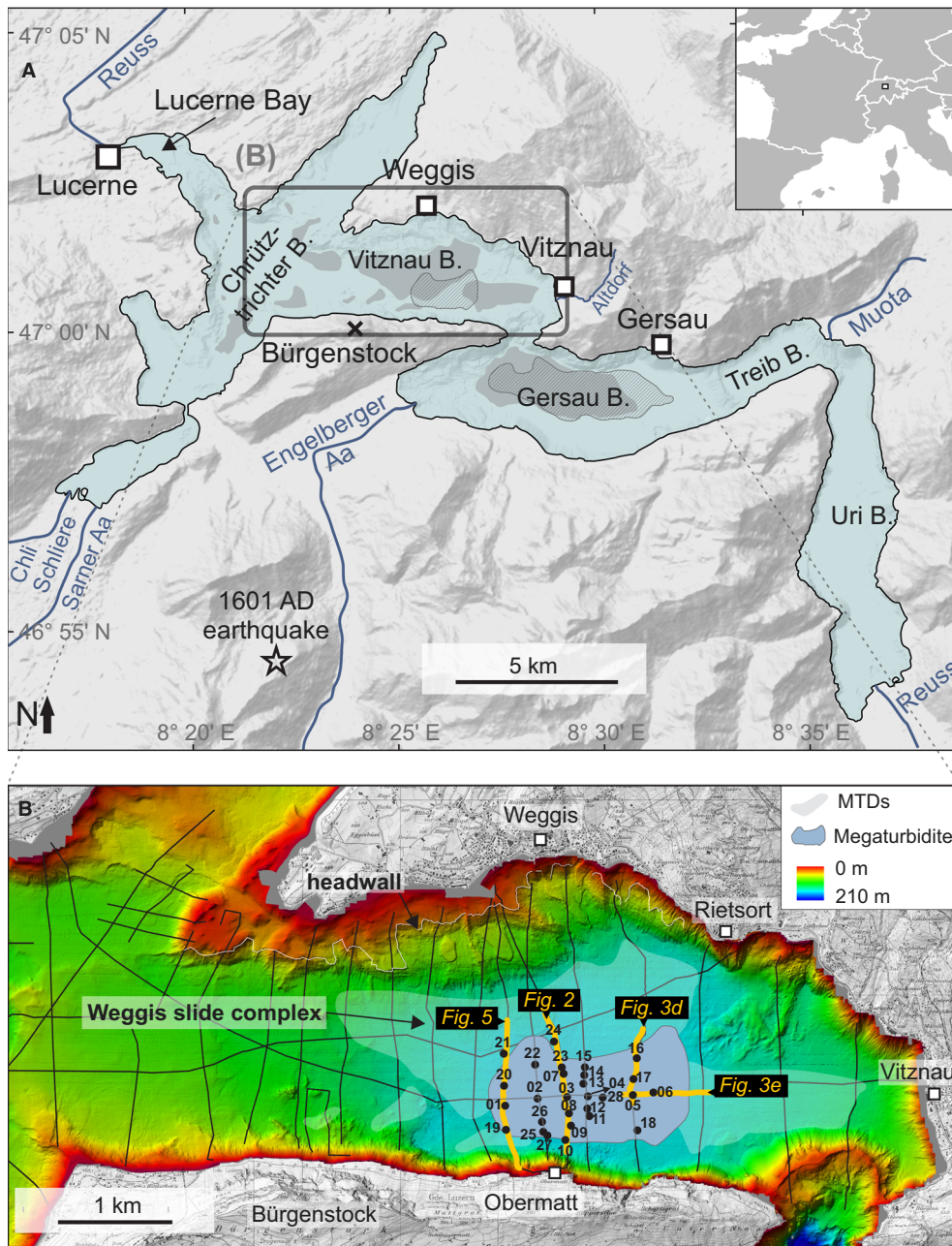
Fig. 1. Overview of Lake Lucerne and surroundings. (A) Map of Lake Lucerne with indication of its different basins, nearby settlements, rivers and the epicentre of the 1601 CE earthquake. The locations of mass-flow deposits (grey shading), megaturbidite (blue shading) and associated sharp headwall (white line) generated by the slope failures in Vitznau Basin triggered by the 1601 CE earthquake (Schnellmann *et al.*, 2006; Hilbe & Anselmetti, 2014). (B) Bathymetric map of Vitznau Basin (Hilbe *et al.*, 2011) with core sites, locations of mass-flow deposits (grey shading), megaturbidite (purple shading), and locations of seismic reflection profiles (profiles in yellow are shown in other figures).

amalgamation has never been demonstrated. Instead, laminations in the megaturbidite base have been attributed to the lake seiche that followed the earthquake, as well as the basin-focused geometry of the deposit, based on three piston cores (Siegenthaler *et al.*, 1987). Since then, new and innovative methods such as X-ray computed tomography (CT) and

palaeomagnetism have evolved and are increasingly used in sedimentology and turbidite research. The 1601 CE Lake Lucerne megaturbidite is revisited by studying 28 sediment cores distributed across the depositional area of the megaturbidite. Combining the new data with existing seismic reflection and bathymetric data allows the reconstruction of megaturbidite deposition with an unprecedented level of detail.

SETTING

Geomorphology and sedimentation at Lake Lucerne

Lake Lucerne is a fjord-like Perialpine lake (total area: 113.6 km^2; surface elevation: 433.6 m above sea level – a.s.l.), located at the northern border of the Swiss Alps (Fig. 1). The lake is part of a series of Perialpine lakes that were formed by glacial erosion and it forms an assembly of several sub-basins that are separated by subaqueous sills and moraines (Hilbe *et al.*, 2011). This article investigates deposits in the Vitznau Basin (maximal depth 150 m). Four major Alpine rivers flow into the lake: the Reuss, Muota, Engelberger Aa and Sarner Aa/Chli Schliere, which all build out deltas at their mouth (Fig. 1). The Reuss outflow is situated in the north-west corner of the lake, where it passes through the city of Lucerne.

Sedimentation in the different sub-basins is generally controlled by the presence or absence of inflowing tributaries. The inflows of the Reuss, Muota, Engelberger Aa and Sarner Aa/Chli Schliere into the different basins result in a considerable clastic input and high sedimentation rates (>5 mm year^{-1}; Siegenthaler *et al.*, 1987; Hilbe & Anselmetti, 2014). The Vitznau Basin on the other hand is relatively isolated from clastic input and is consequently dominated by hemipelagic sedimentation with a relatively slow sedimentation rate (*ca* 0.9 to 1.8 mm year^{-1}; Siegenthaler *et al.*, 1987; Schnellmann *et al.*, 2006). The Vitznau Basin has a thick (>100 m) glaciolacustrine infill and the five to ten uppermost metres are of Holocene age and consist of grey to brown laminated mud with turbidite intercalations, and biochemical varves at the top.

The 1601 CE earthquake and previous work

Since earthquake recording with modern instrumentation, seismicity in central Switzerland has been rather low (Gisler *et al.*, 2004). The most intense earthquake events occurred on: 18 September 1601 (M_w 5.9); 10 September 1774 (M_w 5.7); 7 February 1777 (M_w 5.1); and 14 March 1964 (M_w 5.3; Gisler *et al.*, 2004).

The 1601 CE event near Lucerne has been described in historical documents, and the most reliable and precise report was written by the city clerk of Lucerne, Renward Cysat (Schnellmann *et al.*, 2002; Schwarz-Zanetti *et al.*, 2003). This report contains information about rockfalls, damage and movement of the lake waters after the earthquake. A considerable rockfall took place at the Bürgenstock mountain (Fig. 1) and created additional waves in already wild waters (Schnellmann *et al.*, 2002). Other described events that occurred near the lake include shore collapses and the onshore displacement of floating items up to 4 m above the lake level ('two halbards' high; Cysat, 1601). Parts of land surrounding Lake Lucerne were inundated up to 1 km away from the lake shore ('three gun shots' or 'a thousand steps'; Cysat, 1601). Remarkable was the oscillating behaviour of the Reuss river: over the course of 1 h it flowed back six times into the lake only to return with strong force later. At times of retreat, the river bed was left almost completely dry allowing people to cross by foot at places. Lake shore inhabitants claimed that the waters in the Gersau Basin rose 'as high as mountains' just after the earthquake (Cysat, 1601). The periodic lake level rise and fall could be observed up until eight days after the earthquake in the Uri Basin (Cysat, 1601). These observations imply the generation of a tsunami with maximum wave height of 4 m, followed by seiching of the lake level (Schnellmann *et al.*, 2002). The periodical shut-off of the Reuss outflow indicates that the seiche had an amplitude of 1 to 2 m and a period (one oscillation) of 10 min.

Palaeoseismic investigation of the Lake Lucerne sedimentary infill using reflection-seismic and core analysis revealed that the 1601 CE earthquake triggered major subaquatic mass movements in both the Vitznau and the Gersau basins (Siegenthaler *et al.*, 1987; Schnellmann *et al.*, 2002, 2006; Hilbe & Anselmetti, 2014). The main mass movements in the Vitznau Basin are those of the Weggis slide complex (Fig. 1), which remobilized hemipelagic sediment from the northern slopes, but also smaller mass movements occurred along other slopes (Schnellmann *et al.*, 2002). All of these mass-transport deposits (MTDs) are frontally emergent

(Moernaut & De Batist, 2011) and for the Weggis slide complex the frontal ramp – marking the transition between the confined and emergent part – is clearly visible in the bathymetry (Hilbe et al., 2011) and on seismic reflection profiles (Fig. 2; Schnellmann et al., 2005). The confined part of the MTDs is mostly composed of deformed basin-plain sediments, while the emergent part has been interpreted as mass-flow deposits (Schnellmann et al., 2005; Hilbe et al.,
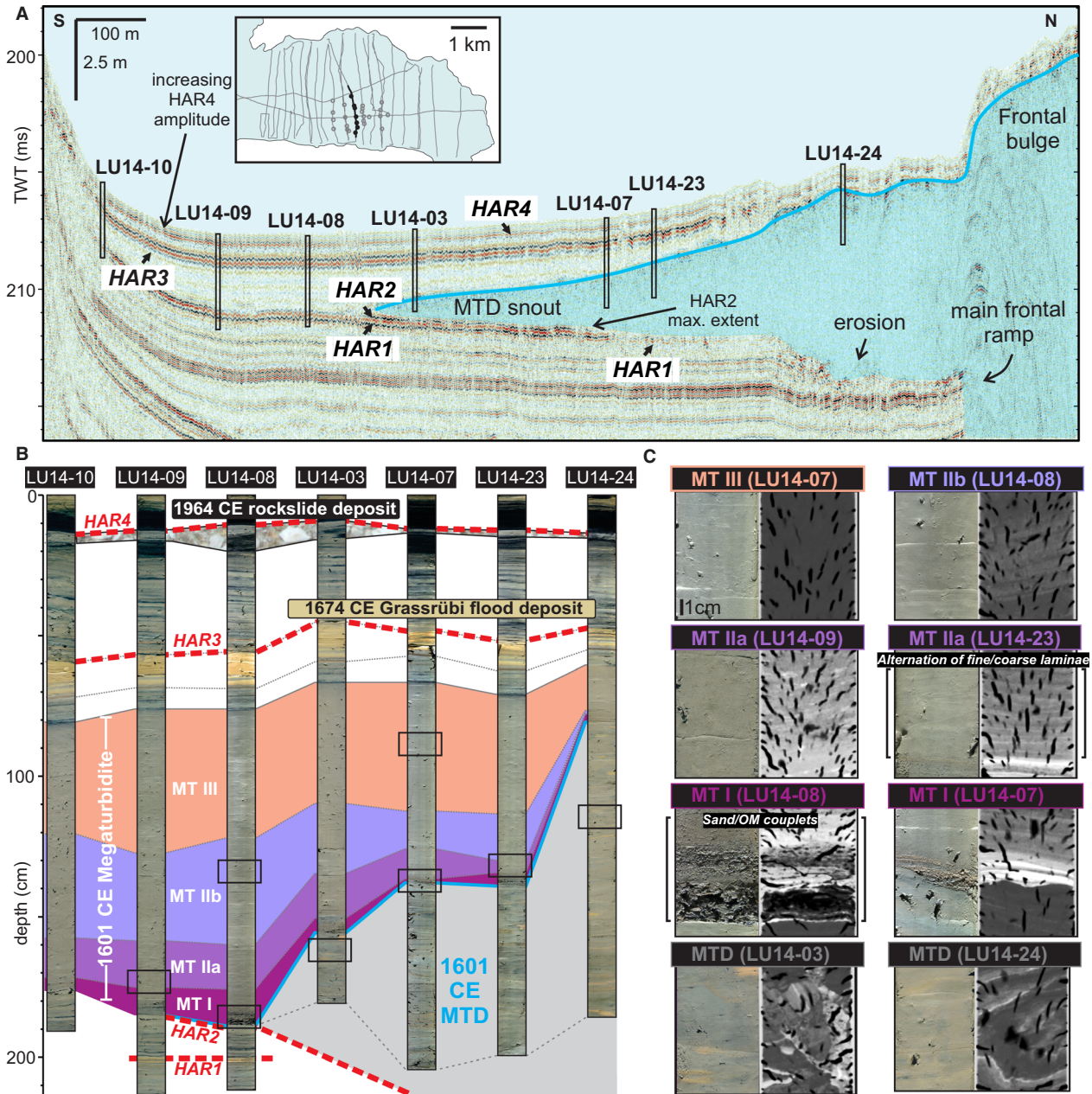
Fig. 2. Overview of sedimentation in the Vitznau Basin and cores along the central north–south seismic profile. (A) Seismic profile (north–south orientation) with indication of core sites and their penetration depth, the interpreted Weggis mass-transport deposit (MTD) (blue) and high-amplitude reflectors (HARs) discussed in this paper. (B) Core photographs of sediment cores along the transect, with correlations of the 1601 CE megaturbidite subunits and other historical event deposits. Beds related to HARs are indicated with red dashed lines. (C) Magnified views of selected core intervals with their corresponding computed tomography (CT) image, illustrating the various sediment types and base of the megaturbidite. Note that the black vertical features represent air pockets that occurred due to sediment degassing upon core retrieval.

2011). The frontal ramp of the MTDs in the Weggis slide complex results in a frontal bulge of up to a few metres in height and thus marks the northern limit of what is at present the deepest part of the basin (Fig. 2).

The main mass movement in the Gersau Basin had a volume almost double of that of the Weggis slide complex and occurred in the western side of the basin from a combination of hemipelagic and deltaic slopes (Hilbe & Anselmetti, 2014, 2015). Numerical simulations of the tsunamis induced by the Weggis and Gersau slides revealed that the mass movement-induced tsunamis can evolve into the observed pattern of seiching with a dominant period of 10 min in the Gersau Basin (Hilbe & Anselmetti, 2015). Also, Siegenthaler *et al.* (1987) previously calculated that the north-western basins (including the Vitznau Basin) have a size for which the natural period is in the order of 10 min, which can be interpreted as a unimodal seiche movement. More recent computational modelling of the tsunami waves predict water-surface displacement of up to 1.5 m and bed shear stresses that were likely capable of remobilizing large amounts of sediments in the Lucerne Bay area (Nigg *et al.*, 2021). Accordingly, in the shallow waters of Lucerne Bay, the tsunami deposit consists of a sharp basal contact with carbonate shell fragments followed upward by a normally graded succession of siliciclastic sand to silt with a high proportion of horizontally bedded wooden particles, indicating a nearshore or onshore source.

METHODS

Seismic reflection and multibeam data

The seismic reflection data, acquired with a 3.5 kHz transducer, has been previously described and discussed in several research papers (Schnellmann *et al.*, 2002, 2005, 2006). The present study describes the acoustic expression of the 1601 megaturbidite in more detail than has been done previously. In particular, the authors investigate whether a series of high-amplitude reflections can be attributed to particular changes in sedimentary characteristics by providing a detailed core-to-seismic comparison. While the seismic reflection data has a relatively high resolution (nominally *ca* 10 cm), it should be taken into account that the core-to-seismic comparison is somewhat uncertain, since a single change in acoustic impedance reflects the

3.5 kHz source signal composed of two or three reflections. Disentangling the sedimentary expression of a series of reflections (for example, related to one or multiple sand–clay transitions) is thus not straightforward. Therefore, the interpretations herein are based on sites where the high-amplitude reflections appear clearly separated from one another on the seismic profiles and then these reflections are traced further in the basin, thereby making the assumption that they remain related to the same sedimentary beds. Bathymetric data and shaded relief shown on the presented maps are retrieved from multibeam data obtained in 2007 (Hilbe *et al.*, 2011).

Sediment coring, handling and logging

Twenty-eight gravity cores (1.5 to 2.4 m length) were retrieved from Lake Lucerne on 26 July 2014 with the research vessel *Thallassa* by means of gravity coring. Core sites were selected in order to form a grid that samples the full spatial extent of the megaturbidite (Fig. 1). Core sites were selected using available seismic data. Sediment cores were divided into sections of maximum 1.5 m for easier transportation and handling. After imaging by means of X-ray computed tomography (CT), sediment core sections were split lengthwise into equal halves and core images were obtained with a linescan camera mounted on the GEOTEK Multi-Sensor Core Logger (Geotek Limited, Daventry, UK).

Computed tomography (CT) scanning

The 1601 megaturbidite was imaged in each (unopened) sediment core with the medical X-ray CT scanner at the Ghent University Hospital (Siemens, SOMATOM Definition Flash; Siemens AG, Munich, Germany). Sediment cores were scanned before core splitting in order to better identify sedimentary structures sampled by the entire core. The applied voltage was 100 kV, with 100 mAs and 0.55 pitch. The across-core resolution of the reconstructed images is *ca* 0.14 mm (detector resolution = 512 × 512 pixels, field of view *ca* 7.0 cm) and down-core resolution (i.e. the thickness of reconstructed slices) is determined by the helix pitch, which is in this case 0.6 mm. The resulting three-dimensional volumes represent the distribution of the radiodensity, or X-ray attenuation coefficients, of the scanned material. X-ray attenuation is function of (average) atomic number and density of the material (Withers *et al.*, 2021).

Dark and light tones indicate materials with low and high radiodensity, respectively. Visualization of the volumes was achieved using the VolumeGraphics VGStudio 3.0 software package. Radiodensity histograms and statistics expressed in Hounsfield Units (HU, a calibrated measure for radiodensity; Hounsfield, 1973) were extracted from a cylindrical volume of interest with a radius of *ca* 2.5 cm along the central axis of the core using the ImageJ software (Schneider *et al.*, 2012). In order to get the best representation of the down-core variations in radiodensity the mode was used, because in contrast to the mean (and median) this statistical parameter is not influenced by the presence of air bubbles (black specks in CT images), which have a very low radiodensity of −1000 HU. To be comparable with the down-core resolution of the grain-size data (see *Grain-size analysis* section), a nine-point running average was applied (i.e. *ca* 0.5 cm) for further analysis.

The µCT imaging (Cnudde & Boone, 2013) was performed at the Centre for X-ray Tomography of Ghent University (UGCT) using the scanner 'HECTOR' (High Energy CT Optimized for Research; Masschaele *et al.*, 2013). HECTOR was specifically designed to scan relatively large samples such as sediment cores, but also allowing to scan small samples at high resolution. An accelerating voltage of 100 kV, with a target power of 10 W, was used for the scans of the complete megaturbidite base in cores LU14-12 and LU14-28. 2401 projections were made, for each projection the detector was illuminated for 0.5 s. The reconstructed voxel size for these scans was 35 µm. The reconstruction of the images was done on the local operation system using Octopus Reconstruction (Vlassenbroeck *et al.*, 2007), and reconstructed volumes were visualized using VGStudio 3.0.

Grain-size analysis

Grain-size analyses of the megaturbidite were performed to quantify downcore grain-size variations within the megaturbidite and spatial grain-size variations across the megaturbidite's depositional area. The sandy base of the megaturbidite was sampled in every core with sample thickness ranging from 0.3 to 0.6 cm, depending on the thickness of specific sand beds. In cores LU14-12 and LU14-28 the complete megaturbidite was sampled with a step-size of *ca* 6 cm and thickness of individual samples of 0.5 cm. In preparation for analysis with a Malvern

Mastersizer 3000 (Malvern Panalytical, Malvern, UK), samples were suspended in 10 ml H_2O. Organic material was dissolved by adding 2 ml H_2O_2 to the suspension, followed by heating on hot plate at *ca* 200°C for 15 min. Subsequently, 1 ml Calgon ($[NaPO_3]_6$) was added and the samples were again heated on the hot plate (5 min at 120°C) to disintegrate aggregates. The samples were then left to cool before analysis with the Malvern Mastersizer. The data produced by the Malvern Mastersizer 3000 were exported and processed with Gradistat v8 for calculation of the different grain-size statistics (Blott & Pye, 2001).

Natural remanent magnetization

A subsample from 19 to 174 cm composite core depth of core LU14-12 was taken with a 2×2 cm U-channel across the three core sections (Weeks *et al.*, 1993). The U-channels were analysed with a 2G 755 SM magnetometer equipped with high resolution pick-up coils and placed in the metal shielded room of the Laboratoire des Sciences du Climat et de l'Environnement in Gif-sur-Yvette (France). The natural remanent magnetization was stepwise demagnetized by alternating field with 12 steps up to 80 mT using the demagnetization coils placed in line with the magnetometer. The characteristic remanent magnetization (ChRM) was determined through a principal component analysis (Kirschvink, 1980). A small viscous component is sometimes present and removed at about 10 mT. The mean inclination value all the way along the studied interval is $68° \pm 7°$, consistent with the location of the core (expected geocentric axial dipole value: 65°). The mean angular deviation (MAD), which is a measure for the accuracy with which the ChRM direction is defined, was calculated on the basis of a minimum of eight steps. The MAD is usually used to determine the quality of the data, but in the case of a turbidite, it may additionally provide information on the settling conditions.

RESULTS

Seismic stratigraphy

Pre-1601 deposits

Below the 1601 CE event deposits, the seismic facies consists of undisturbed, acoustically layered sediment with parallel, continuous
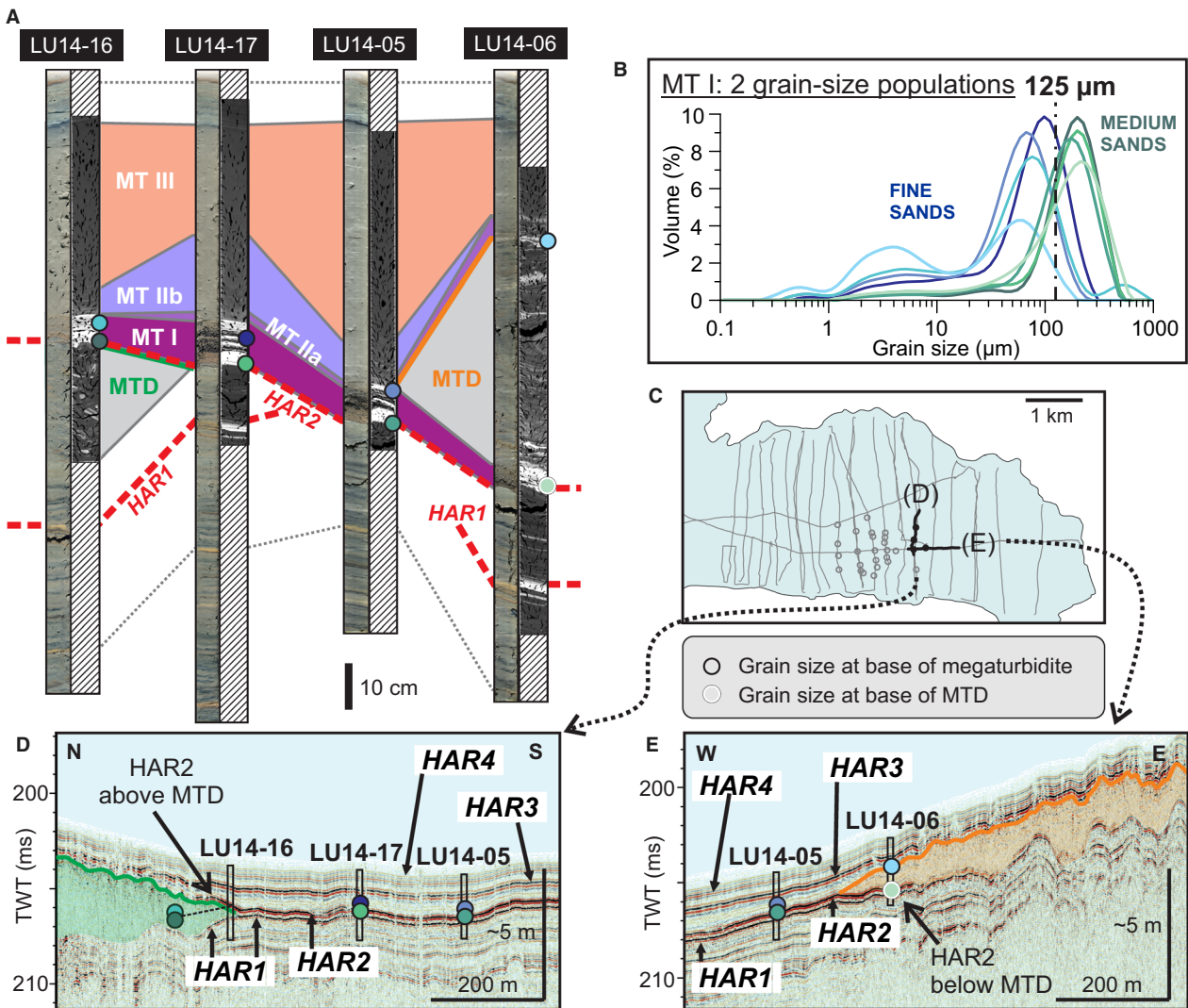
Fig. 3. (A) Sediment core photographs and medical computed tomography (CT) scans along the north–east transect indicated in (C), with correlations of the 1601 CE megaturbidite subunits and beds related to high-amplitude reflectors (HARs; red dashed lines). (B) Grain-size distributions of stacked sandy beds in MT I. Distributions in green correspond to the basal sandy layer [for LU14-06 that is the sand at the mass-transport deposit (MTD) – base], distributions in blue to that of the uppermost sandy layer. The basal sandy layer is characterized by a decrease in sand content from north to south. (C) Overview map indicating the position of the seismic profiles. (D) and (E) Seismic profiles of north–south and west–east transects, respectively, with indication of core sites and their penetration depth. In the North HAR2 sits on top of the eastern Weggis MTD (green), in the East the Vitznau MTD (orange) overran the medium sand bed that causes HAR2.

reflectors. Below the 1601 CE MTDs and megaturbidite, a reflector with relatively high amplitude occurs [High-Amplitude Reflector 1 (HAR1); Figs 2 and 3].

The 1601 CE mass-transport deposits
The MTDs triggered by the 1601 CE earthquake have been described in previous studies as deposits with a transparent-to-chaotic acoustic

facies, a smooth to hummocky surface, basin-ward thinning and abrupt termination (Schnellmann *et al.*, 2002, 2005, 2006; Hilbe & Anselmetti, 2014; Figs 2 and 3). Herein the deposits in the Vitznau Basin are described in more detail, in particular with regard to their stratigraphic position in relation to the megaturbidite. By mapping the distribution of the MTDs in the Vitznau Basin, four main source areas of
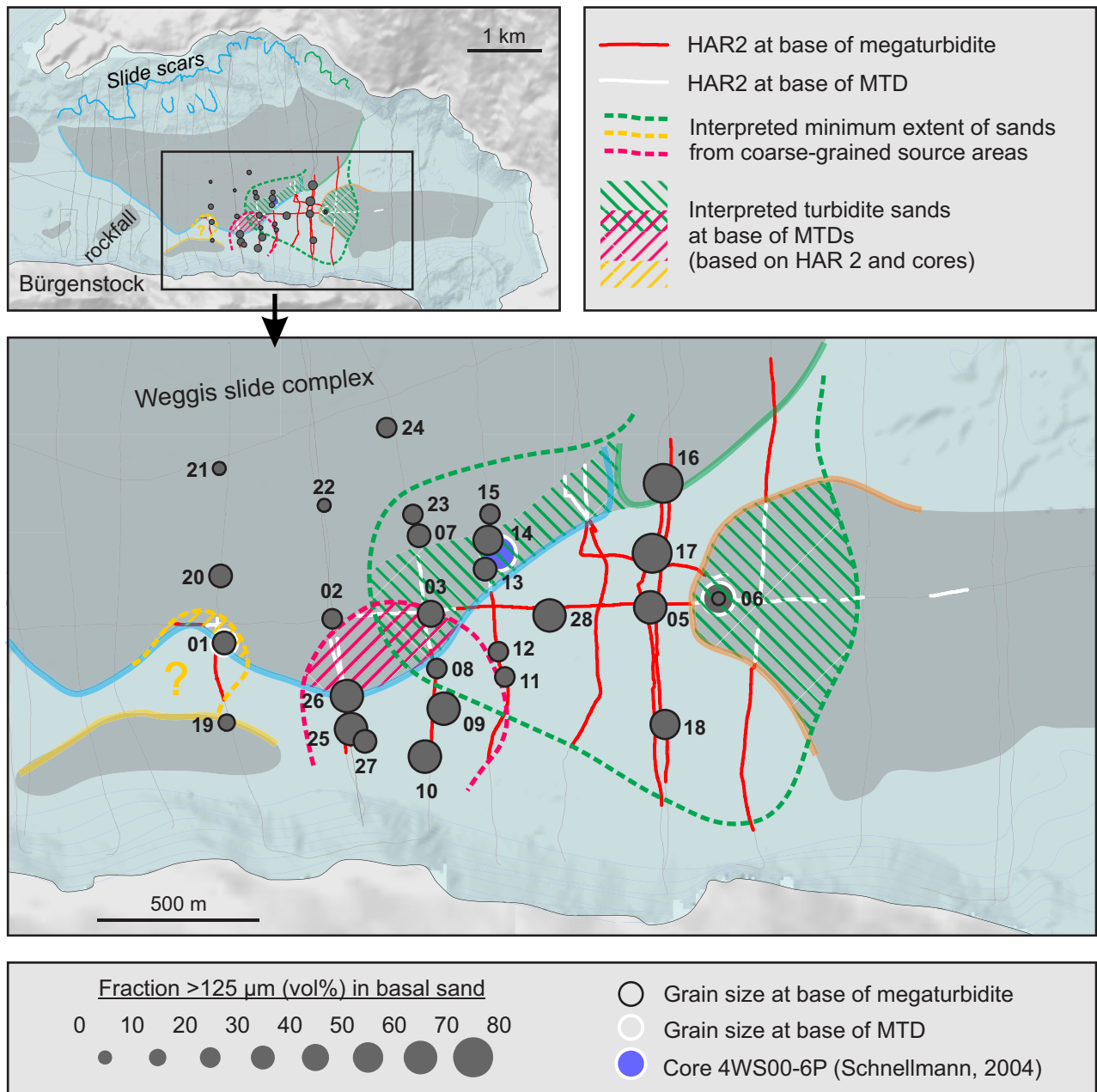
Fig. 4. Overview of grain-size variations at the base of MT I (black circles) or the mass-transport deposit (MTD) (white circles) in relation to the position of MTDs and HAR2. Coarsest grain sizes are associated with HAR2, which is found at the base of the megaturbidite in the central eastern part of the depocentre (red lines) and below the Weggis complex MTD in the central western part of the depocentre (pink lines). Coloured dashed lines represent the interpreted limits of medium sands from specific source areas, with the colour indicating the related MTD. Green indicating a source near Rietsort, pink a source from the steep southern slopes and yellow a southwestern source.

the MTDs can be distinguished (Fig. 4): (i) the northern, gentle slopes, which are the main source of the Weggis slide complex (blue in Fig. 4; Schnellmann *et al.*, 2005; Hilbe *et al.*, 2011); (ii) the steep slopes in the north-east, at the origin of the easternmost deposits of the Weggis slide complex (green in Fig. 4), near Rietsort (Fig. 1); (iii) the slopes north and west of the Nase Moraine in the east (orange in Fig. 4); and (iv) the steep slopes in the south

(western) part of Vitznau Basin, near Obermatt (yellow in Fig. 4).

The central part of the basin is only reached by the emergent part of the MTDs, which have been interpreted as mass flows (Schnellmann *et al.*, 2005; Hilbe *et al.*, 2011). Near the frontal ramp, there are signs of erosion of the underlying sediments by the mass flows on several seismic reflection profiles (Fig. 2), while more distally the mass flows show a conformable contact with the underlying stratified sediments on every profile. The nature of this conformable basal contact, however, differs between MTDs and within one MTD it can change with distance from the snout (i.e. the most distal extent of the MTD). For all MTDs the conformable basal contact is represented by at least a single medium to high-amplitude reflection (HAR1). However, at the snout of several MTDs, a second high-amplitude reflection (HAR2) is present above HAR1. This is the case for the MTDs in the east (sourced from the Nase moraine; orange in Fig. 3) and the Weggis slide complex. In contrast, the snout of the easternmost Weggis slide complex MTD (sourced near Rietsort; green in Fig. 4) does not have this HAR2 at its base, but instead it marks the upper boundary of the MTD, i.e. the contact with the overlying megaturbidite (Fig. 3D).

The 1601 CE megaturbidite
The megaturbidite is characterized in the seismic reflection profiles by semi-transparent acoustic facies, with faint layering parallel to its upper boundary. The megaturbidite is located in the deepest centre of the basin and has a ponded geometry with a maximum thickness of *ca* 2 ms (or *ca* 1.4 m). In its peripheral (mainly northern) parts, it overlies mass-flow deposits, while in its central and southern part it overlies stratified non-event sediments (Figs 2 to 5). Similar to the facies near the snout of several MTDs, the double high-amplitude reflection (HAR1 and HAR2) represents the transition from the layered sediments to the megaturbidite (Figs 2 and 3). HAR1 and HAR2 thus form a continuous reflection wave-train at the base of the MTD–megaturbidite at these locations. The MTD–megaturbidite boundary is in most cases not marked by a prominent reflection and is mainly identified based on the difference in acoustic facies of both deposits (Fig. 2). Only at the snout of the easternmost Weggis slide complex MTD, HAR2 seems to 'intrude' the MTD-megaturbidite complex and thus marks the base of the

megaturbidite covering the mass flow (Fig. 3D). At the south-western extent of the megaturbidite, HAR2 disappears at the snout of a small MTD sourced from the southern slopes (Fig. 5), and thus HAR2 does not mark the upper nor the lower boundary of this MTD.

The post-1601 deposits
The sediments overlying the 1601 megaturbidite have a stratified acoustic facies and a thickness of *ca* 1.1 ms (*ca* 0.70 m). A high-amplitude reflector is present in the lower part of this sequence (i.e. just above the megaturbidite; HAR3) and has relatively constant amplitudes across the basin. In the upper part, the low-amplitude reflections are interrupted by a single high-amplitude reflection that increases in amplitude towards the south/central part of the basin (HAR4; Figs 2 and 3), and highest amplitudes (Fig. S1) near a small post-1601 MTD along the southern slopes.

Sedimentary signatures

Pre-1601 CE deposits
Sediments pre-dating the CE 1601 earthquake event are sampled in the central and southern part of the depocentre, where the megaturbidite does not overlie MTDs, but directly covers laminated 'background' sediments. In most cores, about 20 to 30 cm of sediments pre-dating the CE 1601 event are recovered (for example, LU14-08, LU14-09; Fig. 2). In core LU14-17, about 70 cm of pre-1601 CE deposits were recovered. These sediments generally consist of laminated grey-to-dark grey mud, with intermittent yellow/beige layers consisting of sandy silt (Fig. 3). A prominent set of yellow/beige layers is located about 10 to 15 cm below the megaturbidite and is associated with high radiodensity values (for example, LU14-17 and LU14-06; Fig. 3).

The 1601 CE mass-transport deposits
The MTDs are the result of deformation of originally stratified sediments during sliding and slumping. These event deposits are easily recognizable in cores by their deformed stratification. Here, all cores are retrieved from the unconfined part of the MTDs (i.e. the mass flows), and deformation ranges from a moderate degree of disturbance of the original stratification to a high degree of deformation where sparse signs of the original stratification can be recognized (for example, Fig. 2C). Most MTDs are identified at sites in the northern half of the depocentre, as

suggested by the seismic reflection profiles (Figs 2 and 3). The MTDs belonging to the Weggis slide complex (arriving from the north and north-east) reach deep into the Vitznau Basin and have been sampled in almost half of the cores (Fig. 4). The MTD arriving from the east is sampled at one core site (LU14-06; Fig. 3), as has the MTD that originated from the southern shoreline (near Obermatt; LU14-19; Fig. 5). At most of the coring sites, only the mid to upper part of the MTDs are sampled, but at sites LU14-01, LU14-06, LU14-16 and LU14-19, the bases of the MTDs are reached (Figs 3 and 5). At site LU14-01, the base of the MTD is marked by a 2 cm thick sandy bed with sharp lower and upper contacts (Fig. 5), containing minor amounts of macroscopic organic matter. In LU14-06, the base of the MTD comprises a 4 cm thick bed of medium sands. It exhibits a sharp contact with both the underlying laminated sediments and the overlying deformed muddy sediments of the MTD. In contrast, there is no sand layer at the base of the MTD in sites LU14-16 (Fig. 3) and LU14-19 (Fig. 5), sourced from the north-eastern and southern shorelines, respectively. In these cores the base of the MTD is thus only indicated by the change from horizontally laminated to deformed muddy sediments.

The 1601 CE megaturbidite

The complete megaturbidite sequence is recovered by each of the 28 sediment cores. The sampled thickness of the megaturbidite varies from 10 cm at the edge of the basin (LU14-21) to 136 cm in the centre of the basin (LU14-26). The megaturbidite overlays either layered sediments in the centre of the basin or MTDs at the (mainly northern) periphery of the basin. Overall, above the sharp basal contact, the megaturbidite exhibits a coarse-grained, sedimentologically diverse basal sequence that displays marked variability in terms of composition and grain size (Fig. 6). This diverse basal sequence is overlain by a thick graded unit consisting of sandy to clayey mud that is fairly homogeneous based on macroscopic observations (Fig. 7).

High-resolution grain-size measurements along the megaturbidite are established for cores LU14-12 and LU14-28, and are compared to variations in radiodensity (Fig. 7). This comparison reveals a positive correlation between grain size and radiodensity [expressed as Hounsfield Units (HU)] that is consistent across both cores, and thus suggests that grain size controls radiodensity values. This can be explained by the grain-size

composition of the sediments, which appears to be a mix of two main end members: a clayey silt end-member with a mode of *ca* 5 µm and a coarse silt to sand end member with a mode of >40 µm (Fig. 7). There is a consistent trough in the grain-size distributions at *ca* 16 µm that separates these end-members, and more input of the coarse fraction (>16 µm) into the fine muddy matrix (<16 µm) seems to result in the higher modal radiodensity (Fig. 7). This is likely due to a combination of poorer sorting – resulting in a better packing and higher density – and higher effective atomic number of the coarse silt and sand grains compared to organic muds. Radiodensity in these cores is thus predominantly controlled by grain size (more specifically the >16 µm fraction), and the relation between both parameters established from cores LU14-12 and LU14-28 allows us to use the radiodensity as a proxy for grain size in all other cores.

The megaturbidite was subdivided into three subunits (MT I, MT II and MT III), based on grain size, palaeomagnetic properties and sediment structure (Fig. 7). Subunit boundaries were determined using fixed radiodensity thresholds, allowing spatial mapping of the different megaturbidite subunits. In the following sections the sedimentary characteristics and spatial distribution of each subunit are described.

MT I: Sandy base. Macroscopic observations, grain-size analysis and CT-scans reveal that the base of the megaturbidite generally consists of coarse silts to sands. These megaturbidite bases often exhibit distinct sand layers, separated by finer-grained or organic-rich layers (Figs 6 and 8), but with an overall fining-upward signature. In LU14-12, at the transition from 'background' laminated sediment to the sandy megaturbidite base, ChRM remains stable (illustrated by the declination in Fig. 7) with however an increase in MAD values, indicating that the signal is not as well defined as below. This is most likely due to the presence of coarse, more unstable, magnetite grains in this horizon. The first subunit (MT I) is defined as consisting of more than 50% of the coarsest end member (i.e. >16 µm), which corresponds to a radiodensity of >750 HU, although values are often lower in the intercalated fine-grained or organic layers. Grain-size analysis of the MT I deposit in all cores reveals that there are two grain-size populations in MT I: medium sands that are generally coarser than 125 µm (further named medium sands), and coarse silts to very fine sands with a mode
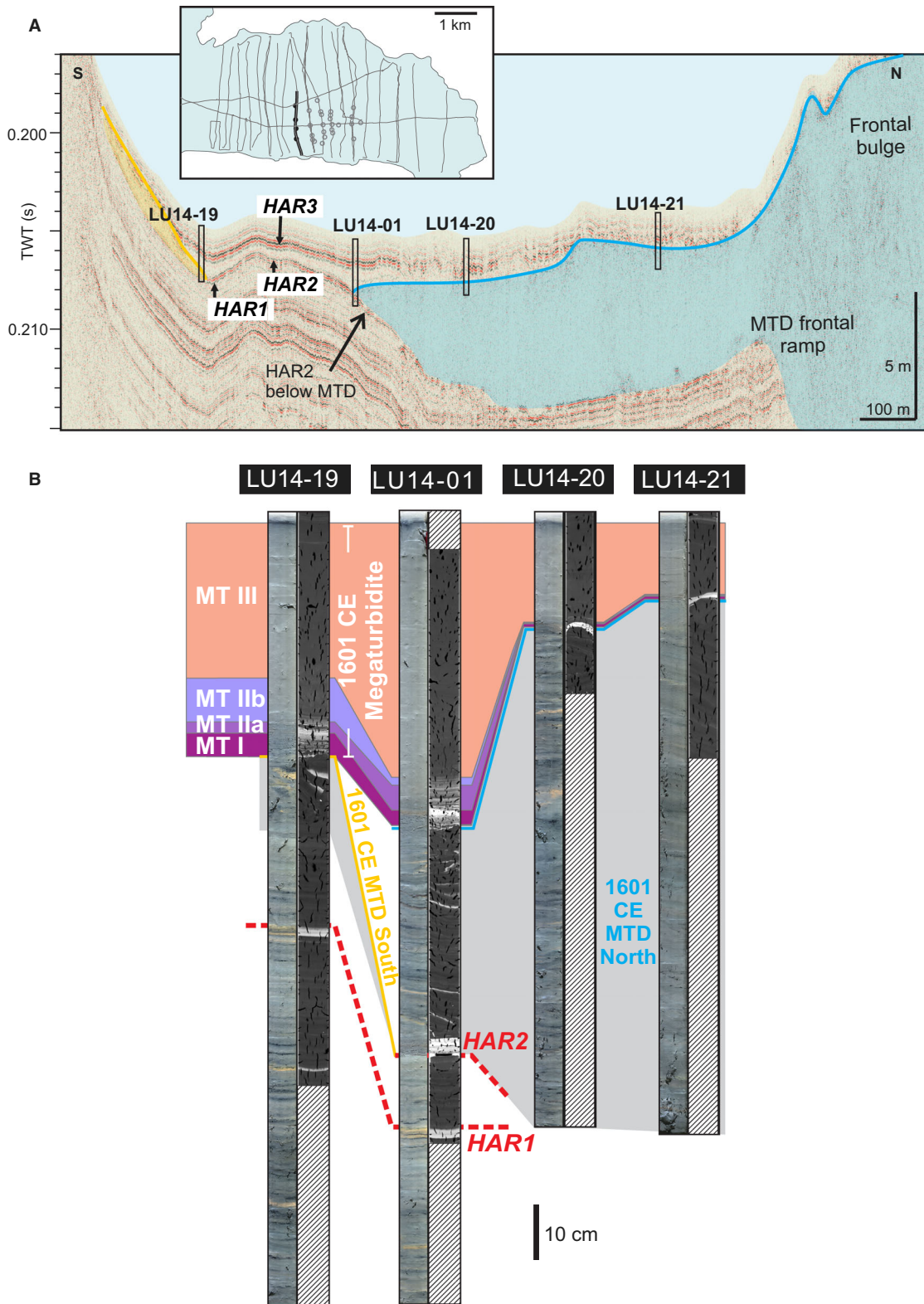
Fig. 5. (A) Seismic profile along most western north–south transect with indications of core sites and their penetration depth. (B) Core photographs of cores along transect together with medical computed tomography (CT) images, with correlations of the 1601 CE megaturbidite subunits and beds related to high-amplitude reflectors (HARs; red dashed lines). In the South (LU14-19) HAR2 is absent, in the North (LU14-01) the Weggis mass-transport deposit (MTD) (blue) overran the medium sand bed that causes HAR2.

© 2023 The Authors. *Sedimentology* published by John Wiley & Sons Ltd on behalf of
International Association of Sedimentologists., *Sedimentology*, **70**, 1496–1520

<125 μm (further named fine sands; Fig. 3B). While in some locations layers with medium sands are covered by a layer with fine sands, other cores contain only fine sands. The distinct organic-rich layers, which are present in nine out of the 28 cores, consist of (parts of) twigs and leaves within a matrix of mud clasts and medium sands (Fig. 8). Based on the μCT images, the leaves and twigs (up to several centimetres in length) amount for *ca* 50% of these organic-rich layers. The mud clasts (*ca* 45%) have a diameter that is generally below 1 mm, but can be up to several millimetres in size. The grain size of the matrix sands (*ca* 5%) is similar to that of the underlying and overlying medium-sand layers – as determined from a visual inspection of the μCT images. Apart from the distinct organic-rich layers, some laminae composed of mud clasts or mud clasts with some organic remains (mostly leaf fragments) occur within the sand layers, always with a medium-sand matrix. For example, in both LU14-12 and LU14-28 such a mud-clast lamina occurs near the top of the lowermost sand layer (Fig. 8), while the second-from-below sand layer has some laminae with mud clasts, leaf fragments and an occasional twig. The nine cores that contain these couplets of medium sand and organic material (further referred to as a 'sand/OM couplet') are mostly aligned in a north-east/south-west direction between the north-eastern end of the megaturbidite and its depocentre (Figs 6 and 8). Only cores LU14-15 and LU14-23 are exceptions to this trend, as they are located along the northern border of the megaturbidite, and thus separated from the other cores with sand/OM couplets by several cores that do not have these. In the north-east, it is striking that cores LU14-05, LU14-16 and LU14-17 all contain medium sands at the base of MT I, but this is not the case for the nearby LU14-06, where MT I consists of fine sands but a thick layer of medium sands forms the base of the MTD (Fig. 3). The fine sands at the base of MT I in LU14-06 correspond in grain size to the upper MT I sand layer in cores LU14-05, LU14-16 and LU14-17, as well as the MT I grain size in many other cores to the

west (Fig. 4). Hence, while the medium sands continue below the MTD in LU14-06, the fine sands cover it (Fig. 3A). Furthermore, the medium sands in this north-eastern end show a subtle fining trend towards the south-west, whereas the fine sands show a subtle fining trend to the north-east (Fig. 3B). The majority of the MT I sequences contain more than one sand layer and cores with sand/OM couplets consistently show three or four sand layers (Fig. 6). However, the upper (fine) sand layer never has an associated organic-rich layer on top, and thus cannot be regarded as a sand/mud couplet.

The spatial distribution of MT I is rather heterogeneous, and is thickest in the south-central to south-western part of the megaturbidite (Fig. 9), where the water depth at time of deposition was largest. However, there is a second MT I depocentre in the north-east, confined between the eastern MTDs, and especially in the central-eastern part there appears to be a negative relationship between MTD presence and MT I thickness (Fig. 9). Finally, along the northern border of the megaturbidite, LU14-15 and LU14-23 have a relatively thick MT I. The increased MT I thickness in the north and north-east seems to correlate with the presence of sand/OM couplets (Fig. 6).

MT IIa and MT IIb: Graded silt. MT II is distinguished from MT I by its finer grain size, comprising silty to sandy mud (Fig. 7). The subunit is characterized by a general fining upcore trend and declining MAD values (in LU14-12). MT II was subdivided into two parts (MT IIa and MT IIb) based on grain size, although these two subdivisions also show differences in sediment structure.

MT IIa is coarser grained than MT IIb and consists of sandy mud with >25% of the coarsest (>16 μm) end-member, corresponding to a radiodensity of >605 HU (Fig. 7). In LU14-12, MAD values are high and declination remains stable. MT IIa shows a general fining-upward trend in all cores, but the sediment structure may vary between cores. In the depocentre, MT IIa shows mainly a strong and consistent

Fig. 6. Core photographs and medical computed tomography (CT) images of the base of the megaturbidite (MT I) at each core site, illustrating the amalgamation/stacking of turbidite sands. Vertical black scale bars are 5 cm. The inset map displays the distribution of cores with couplets of medium sand and organic material (sand/OM couplets) at the megaturbidite base (green-filled circles), together with the number of sandy layers at the megaturbidite base ('pulses'), indicated by the number in the circles. Numbers next to the circles indicate the core names (without the 'LU14-' prefix).
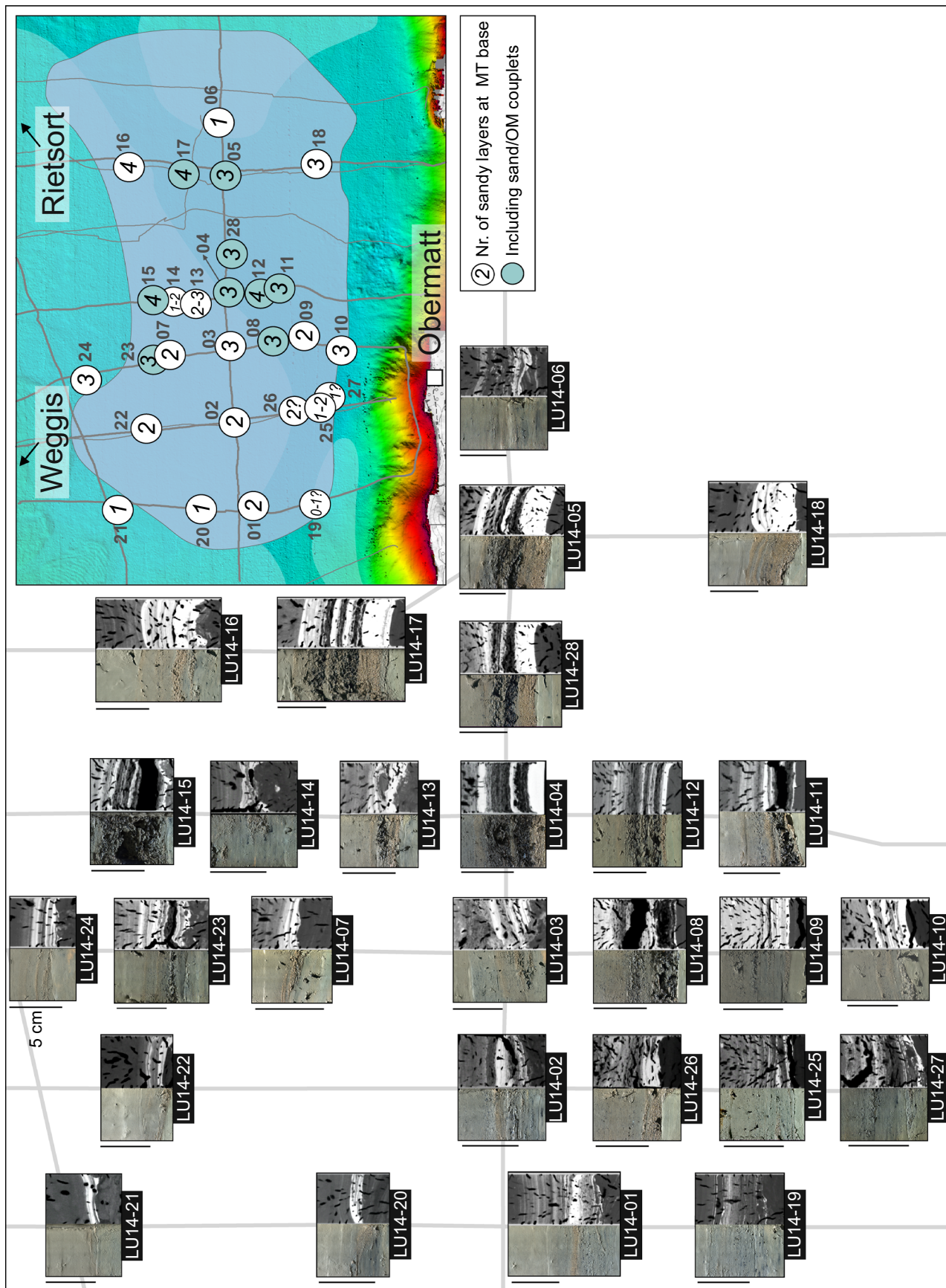
upward grading, while towards the periphery a mix of graded, homogenous, mottled and layered sedimentary structures characterize this subdivision. In particular, MT IIa displays pronounced alterations of coarser and finer-grained laminae at its periphery, where it reaches a thickness of merely a few centimetres (Fig. 9). The alterations of coarser and finer laminae overlying the sandy layers of MT I are best visible in the CT images of cores LU14-01, LU14-07, LU14-16, LU14-23, LU14-25, LU14-26, LU14-27, and arguably LU14-11 and LU14-12 (Fig. 6). Note that these alternating laminae are too subtle to be observed macroscopically, but are distinct in the (μ)CT data (Fig. 8 and 9B). The spatial distribution of MT IIa is strongly focused to the depocentre of the megaturbidite, which was the deepest part of the basin at time of deposition, and is thus thickest in the south (Fig. 9).

MT IIb consists of mud with 20 to 25% of the coarsest (>16 μm) end-member and the sandy component is barely present (<3% very fine sand). This corresponds to a radiodensity of 540 to 605 HU. The MAD values continue to decline steadily to reach a minimum at the top of the subdivision (Fig. 7), and declination varies in this interval, reaching values similar to the 'background values' towards the top of MT IIb. Macroscopic observations reveal little sedimentological variation within this unit, but grain-size measurements and CT data show a general fining-upward trend with superimposed subtle grain-size variations (Fig. 7). Similar to MT IIa, but at fewer locations and at shallower water depths, fine laminations are observed near the base of the sub-unit and grade into homogenous mud (LU14-01, LU14-16 and arguably LU14-20) where MT IIb is merely a few centimetres thick. This occurs more in the peripheral areas of the megaturbidite compared to MT IIa, because MT IIb shows a less basin-focused distribution (Fig. 9).

MT III: Homogenous clayey mud. MT III is characterized by its very fine grain size (clayey mud; <20% of the coarsest end member; <2% very fine sand and <540 HU) which remains stable or has a very subtle fining-upward trend, without superimposed grain-size variations nor any sedimentary structures. This pattern is also reflected in the declination and MAD values of LU14-12, which remain stable (Fig. 7). The transition from MT II to MT III is gradual. Spatially, the MT III division is present in all cores, and thus shows a much more draped distribution compared to the other divisions (Fig. 9).
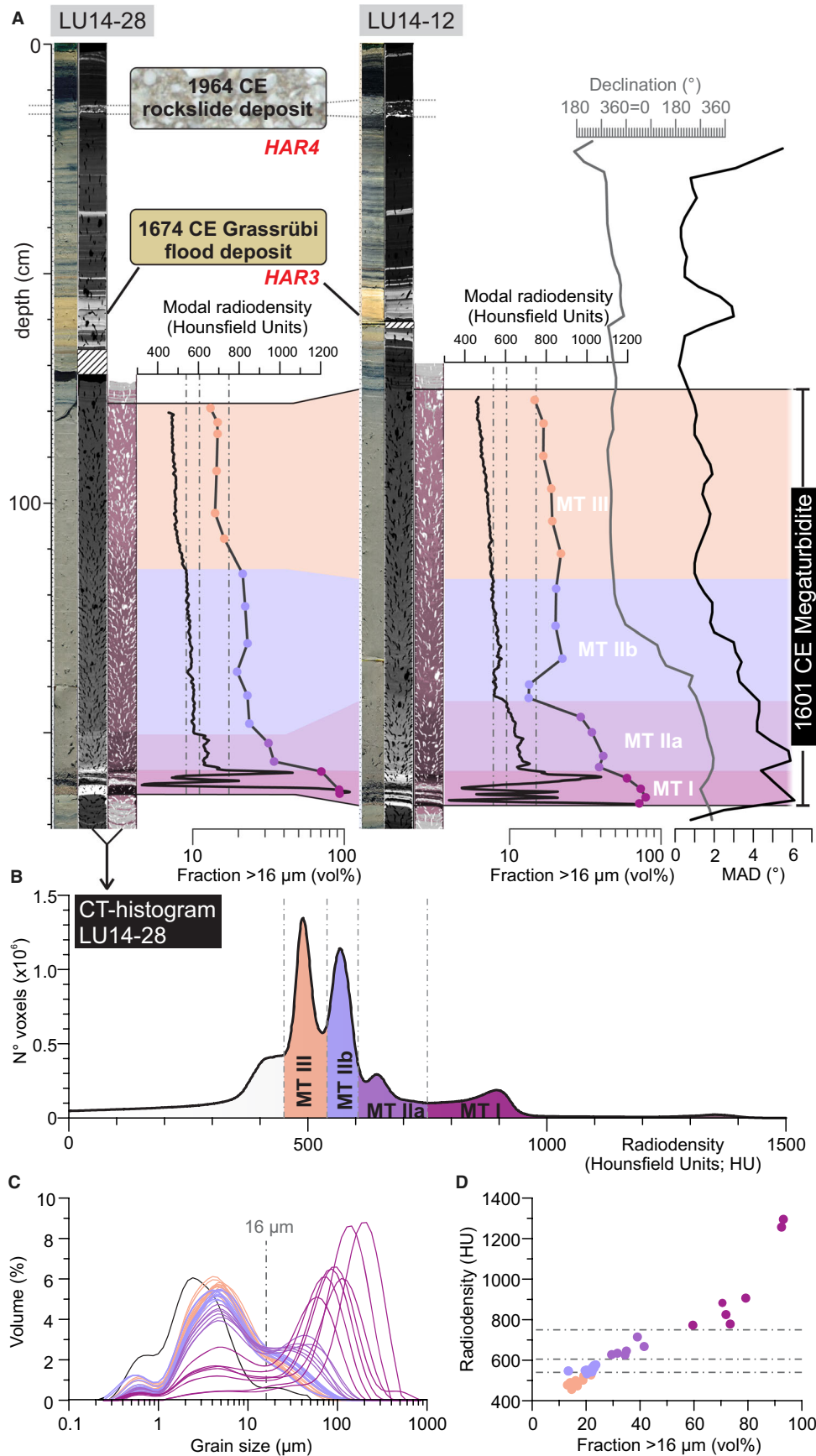
Post-1601 deposits
The 1601 megaturbidite is overlain by 70 to 80 cm of mostly grey, layered muds (Fig. 7). Approximately 10 to 15 cm above the top of the megaturbidite a 10 to 15 cm thick interval of yellow-brown, laminated sandy mud with a high radiodensity occurs (Fig. 7; 55 to 66 cm core depth in LU14-28). Around 15 cm core depth, a grey layer with coarse sands and gravel is present. The thickness of this layer is spatially variable and coarsens towards the southern shore, where it consists of a 20 cm thick mud-clast conglomerate that includes gravel and pebbles (LU14-11, Fig. S1). Towards the northern shore this layer is merely a centimetre thick and shows a graded appearance. Black, finely laminated sediments occur between 5 cm and 20 cm core depth. In the southern part of the basin these laminations are interrupted by the grey, coarse layer, described above. In the upper 5 cm, sediments consist of brown mud (Fig. 7).

DISCUSSION

Core-to-seismic correlation

Core-to-seismic correlation allows discerning the sedimentological nature of the high-amplitude reflections, which is key to reconstructing the events that took place following the 1601 CE earthquake. The sedimentary facies that consists of deformed mud corresponds to the 1601 CE MTDs identified on the seismic reflection profiles, which confirms that these deposits are indeed the result of mass-wasting processes (Fig. 2). The semi-transparent nature of the

Fig. 7. Analyses on master cores LU14-28 and LU14-12. (A) core photograph, medical computed tomography (CT) scan and colour adjusted CT scan with grain size (fraction >16 μm), modal radiodensity and palaeomagnetic measurements (MAD = mean angular deviation). Yellow squares indicate the position of μCT scans presented in Fig. 8. (B) Histogram of radiodensity of the LU14-28 core, with indication of the range of values corresponding to different megaturbidite sub-units. (C) Grain-size distributions of all LU14-12 and LU14-28 grain-size analyses with colours indicating the sub-unit. (D) Scatterplot of radiodensity versus grain size showing a clear positive correlation. Horizontal dash-dot lines indicate threshold radiodensity values between sub-units.

© 2023 The Authors. *Sedimentology* published by John Wiley & Sons Ltd on behalf of
International Association of Sedimentologists., *Sedimentology*, **70**, 1496–1520

megaturbidite on seismic profiles is the result of the relatively homogenous silty mud that comprises the largest part of the megaturbidite and mostly lacks internal layering (Schnellmann et al., 2002, 2006).

The high-amplitude reflections HAR1 and HAR2 are spaced close together and determining their exact sedimentary nature is therefore difficult at most sites. However, at site LU14-16 these reflections appear separated from one another by an MTD (Fig. 3A and D). From core LU14-16 it thus appears that the lowermost high-amplitude reflection (HAR1) is the result of a change in acoustic impedance occurring within the layered 'background' sediments, located below the megaturbidite, pre-dating the CE 1601 earthquake. The HAR1 is thus likely related to a yellow layer with high radio-density, for example clearly visible in core LU14-16 and confirmed by LU14-17 (Fig. 3A and D). The HAR2, located above the mass-flow deposit at LU14-16, appears to be related to the thick medium sand layer at the base of the megaturbidite (LU14-16; Fig. 3A and D). Tracking this reflection further into the basin, it appears that, where the megaturbidite base is marked by HAR2, the cores consistently reveal a relatively thick basal medium sand bed (several centimetres thick, mostly >50% of >125 μm) comprising organic material. In

contrast, in cores where HAR2 continues beneath the MTD (if present) a medium sand layer is absent at the base of the megaturbidite but instead observed at the base of the MTD, for example, LU14-01, LU14-06 and 4WS00-6P (Schnellmann, 2004; Schnellmann et al., 2006; Figs 3 to 5 and Fig. S1). Therefore, HAR2 is attributed to a medium-grained sand bed at the base of the megaturbidite that is also found underneath the eastern-derived MTD present at LU14-06 (Fig. 3A to E).

Above the megaturbidite, two high-amplitude reflections can be discerned in the seismic reflection profiles: HAR3 and HAR4. Similar to HAR1, HAR3 appears to be related to coarse, yellow/beige sandy layers, which in this case are found above the megaturbidite and are present in all cores. These turbidites were deposited following the 1674 CE Grassrübi landslide (Figs 2 and 7). The landslide blocked the Altdorf stream (Fig. 1) and subsequent floods eroded the onshore landslide, depositing this material as turbidites in Vitznau Basin (Schnellmann et al., 2006; Louis et al., 2008). The yellowish/beige colour is due to high iron content of the sandstone and marl that are found in the source region of the landslide ('subhelvetic units'; Schnellmann et al., 2006; Louis et al., 2008).

The reflection amplitude of HAR4 varies spatially, with increasing values towards the
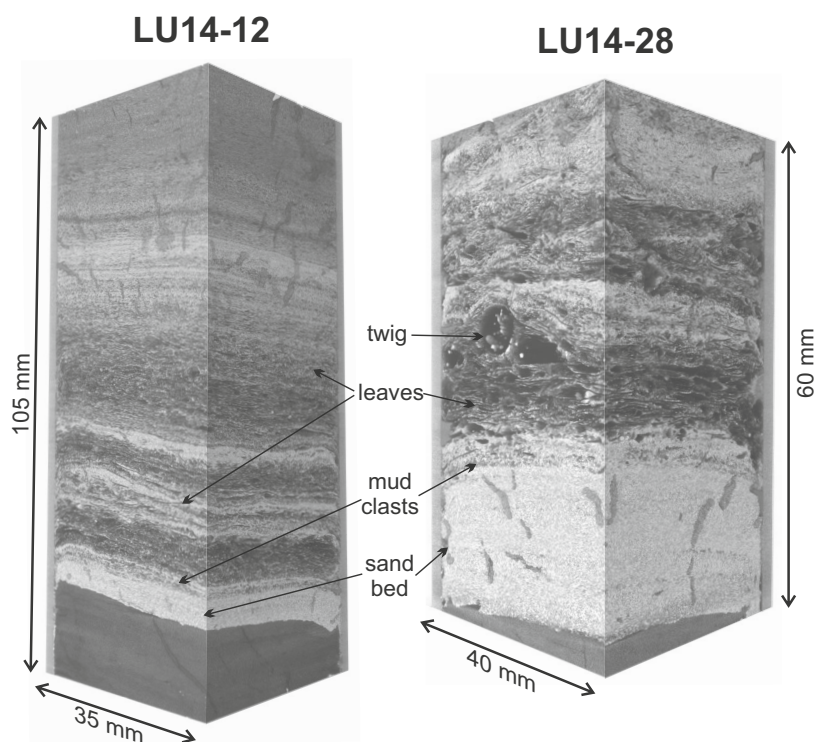
Fig. 8. X-ray computed microtomography (μCT) images of the megaturbidite base in LU14-28 (left) and LU14-12 (right) obtained using HECTOR (High Energy CT Optimized for Research). Both cores reveal stacked sandy turbidite beds (white), intercalated with layers consisting of organic material (black) and mud clasts (grey tones) in a sandy matrix (sand/OM couplets).
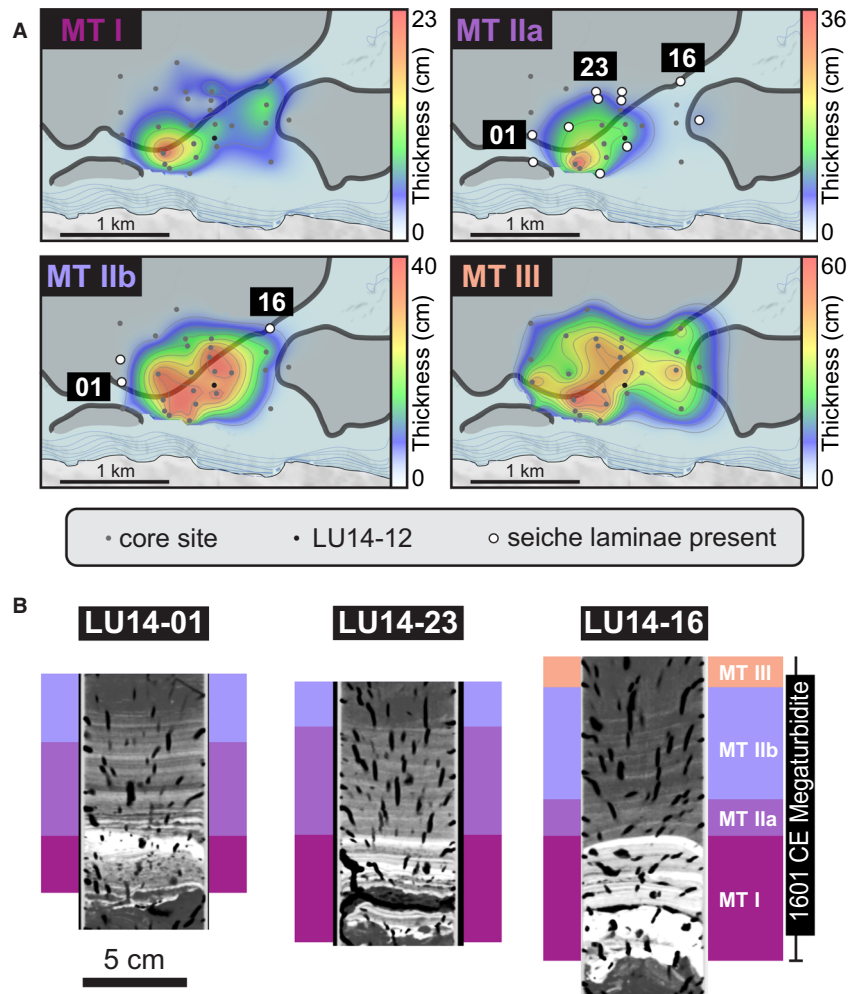
Fig. 9. (A) Thickness maps of the megaturbidite sub-units in Vitznau Basin. Grey areas mark the extent of mass-flow deposits. MT I comprises stacked (sandy) turbidite beds with variable thicknesses throughout the basin, reflecting turbidity currents arriving from different sides of the basin. MT II-III reflect the fine units (silty mud) of the megaturbidite, and shows the evolution from sedimentation focused in the basin centre (MT IIa) to basin-wide sediment draping (MT III). (B) Magnified views of medical computed tomography (CT) scans of the megaturbidite base illustrating seiche laminae in MT IIa and MT IIb.

south/central part of the basin and reaching a maximum near an MTD located along the southern slopes (Fig. S1). This MTD is located higher in the stratigraphy than the 1601 CE deposits (Fig. S1) and is known to have evolved from a rockfall event in 1964 in a quarry at Obermatt (Schwarz-Zanetti *et al.*, 2003, Fig. 1B). Hence, HAR4 is most likely the sedimentary expression of the blue-grey graded turbidite that evolved from that event, interrupting the darker biochemical varves reflecting the lake eutrophication since the mid-20th century (Schnellmann *et al.*, 2006; Louis *et al.*, 2008). At sites proximal to the rockfall this layer contains pebbles and rock fragments (Fig. S1).

Deposition of mass-transport deposits and amalgamation of sandy turbidity currents (MTD and MT I)

The deposition of multiple MTDs and the high sedimentological variability at the base of the

megaturbidite suggest a potential interaction between different sandy turbidity currents travelling towards the centre of the Vitznau Basin. Therefore, the timing of MTDs and turbidite deposition were explored using sedimentological characteristics and core-to-seismic comparison.

Mass-transport deposit–turbidite stacking

The occurrence of macroscopic organic material within the sandy base of the megaturbidite (Figs 6 and 8) implies a very shallow and near-shore source area for these deposits, likely an area not far from the 1601 CE lake level, where coarse sands and organic remains would have initially accumulated. Some of the shallowest slide scars identifiable in the Vitznau Basin are located in the north-eastern part of the basin (Fig. 1B), and this area is therefore considered as a possible candidate for the source area of the sand/OM couplets. This interpretation is supported by the spatial distribution of the cores

with sand/OM couplets, because these are mostly aligned in a north-east/south-west direction (cfr. LU14-04, LU14-05, LU14-08, LU14-11, LU14-12, LU14-17 and LU14-28, Fig. 6), with the thickest and coarsest deposits located in the north-east. Furthermore, the lowermost sandy layer in these cores can be correlated across the central-eastern part of the basin and exhibits a similar grain-size distribution in the different cores, albeit with a subtle decrease in the coarse sand fraction from north-east to south-west, further supporting a north-eastern source (Figs 3B and 4).

The multiple sand/OM couplets correspond to HAR2 and can be traced across the basin (Figs 2 to 6). This implies that the medium sand bed found at the base of the MTD at site LU14-06 represents one of the turbidites with a north-eastern source area. Indeed, this layer contains coarse organic material, confirming its association to the sand/OM couplets (Fig. 3). Moreover, the grain-size distribution of this layer is also similar to the turbidites arriving from the north-east (Fig. 3). The MTD overlying this turbidite at site LU14-06 can be linked to slope failure in the eastern part of the basin, near Vitznau. The sequence of deposits at site LU14-06 thus indicates that at this location first a turbidity current arrived from the north-east (near Rietsort), which was then overridden by a debris flow arriving from the east (near Vitznau). In the same way we interpret the sand at the base of the MTD in core 4WS00-6P from Schnellmann (2004; Figs 4 and S1) to be originating from a north-eastern (Rietsort) source, after being overridden by the MTDs of the Weggis slide complex originating from the northern slopes. Because this sand is interpreted to be associated with HAR2, the authors conclude that the entire area where HAR2 is present below the eastern Weggis slides (Figs 2, 4 and 5) has undergone stacking of the Weggis MTDs on top of north-eastern-sourced turbidite sands. Indeed, the cores retrieved in the Weggis slides that are located on top of the area where HAR2 forms the base of these slides (i.e. LU14-03, LU14-13, and arguably LU14-07 and LU14-14) do not have these sand/OM couplets. However, the cores just north of these (i.e. LU14-15 and LU14-23) do have sand/OM couplets in MT I. Hence, we observe stacking of the north-eastern-sourced turbidite sands on top of the Weggis MTDs, and attribute this to the later arrival of the Rietsort turbidity currents at these locations. The absence of a clear HAR2 at these locations is probably related to the thinner and finer-grained nature of

MT I, which is a result of the relative shallowness of these locations following MTD deposition (Fig. 2).

At site LU14-01, in the south-western part of the basin, there is evidence for the first arrival of a turbidity current originating from the south (near Obermatt), which is then overridden by a debris flow and turbidity current arriving from the north (Weggis). The lower turbidite sand related to HAR2 is wedged between underlying laminated sediments and an overlying MTD (Fig. 5), a sequence similar to that observed at sites LU14-06 and 4WS00-6P. Based on the distance of the core location to the nearby slope failures, it can be expected that a turbidity current from the south or south-west (where the Bürgenstock rock slide reached the lake, Fig. 4) would have arrived earlier than a debris flow originating from the northern side of the basin. Therefore, it is interpreted that at site LU14-01, first a sandy turbidite arrived from the south (west), which was then overridden by a mass flow and another turbidity current from the north, associated with the Weggis slide complex.

Turbidite pulses, stacking or banding?

In the context of subaqueous palaeoseismology, distinct grain-size variations at the base of a single event deposit ['multi-pulsed turbidite' (Van Daele et al., 2017)] are commonly interpreted as having been deposited by either a multi-pulsed single flow (Goldfinger, 2009), or by multiple flows that were coevally triggered in different source areas and which converge downstream (Nelson et al., 2012; Van Daele et al., 2017). However, the megaturbidite base in Lake Lucerne is in some places sedimentologically very similar to what has been described as 'turbidite banding' in deep-sea sedimentary sequences (Stevenson et al., 2020), in particular because of the presence of organic rich layers with mud clasts. Turbidite banding is defined as the alteration between 'clean' fine sand bands and mud rich (45 to 75%) bands. Such deposits are interpreted to form progressively in the upper-stage plane-bed flow regime via tractional reworking beneath mud-laden transitional plug flows (Baas et al., 2009, 2016) and does not imply flow pulsing (Stevenson et al., 2020). This study further explores whether these processes can be distinguished based on sedimentological characteristics and their distribution in the basin.

The sand/OM couplets in MT I, which were attributed to a source near Rietsort, consistently

occur in sets of two or three couplets (covered by a fine sand layer). Also in LU14-16, the core nearest to the Rietsort source area, MT I contains two or three medium-sand layers, albeit without an associated organic-rich layer. The organic macroremains thus seem to bypass this proximal location and are instead thickest in the most distal locations (LU14-04 and LU14-08; Fig. 6), whereas the medium sand layers become thinner. Apart from the consistency in the number of couplets, the similarity of the lower two sand layers between cores LU14-12 and LU14-28, located *ca* 200 m apart, is remarkable. While the lowermost sand layer is much thicker in LU14-28, this sand layer has a particular mud-clast lamina near its top in both cores (Fig. 8). The second sand layer has several organic-rich laminae in both cores. Combining these observations, the authors believe that turbidite banding through tractional reworking – or any other process – in a single flow is an unlikely cause for the couplets, because this would result in a much more spatially variable pattern. Especially in northern (lateral to the main flow) core locations LU14-15 and LU14-23 one would expect very different flow regimes and thus not the same type of banding. Instead it is proposed here that each sand/OM couplet is linked to a pulse in the turbidity current that may result from either lateral failure propagation (e.g. L'Heureux *et al.*, 2014) or synchronous failure on at least three along-slope sources. The latter interpretation is substantiated by the three distinct convex headwalls that have been identified on the steep Rietsort slopes (Hilbe *et al.*, 2011).

Nevertheless, three separate flows do not explain the segregation that was observed between the sand and each overlying organic-rich layer. Given the medium sandy matrix in the organic-rich layers, the authors propose that the OM – which was mixed with the sand at the source location – and the mud-clasts – which have been entrained during the flow – are floating on top of a basal laminar flow, similar to large floating clasts as described by Postma *et al.* (1988), but here facilitated by the lower density compared to the sand grains. In the western part of the megaturbidite, the nature of the MT I sequence is somewhat different than the thick sequences found in the central/east central part. Here only one or two sandy layers are usually present, with no organic-rich layers separating them, overall an increase in pulses from the north-west to the south-east (cores LU14-01, LU14-02, LU14-19, LU14-22, LU14-25

and LU14-27; Fig. 6) and up to three pulses in the (south)central part of the basin (LU14-03, LU14-09 and LU14-10). This probably points to a north-western source of the westernmost, uni-pulsed sandy layers (LU14-20 and LU14-21), which eastward became amalgamated with other turbidite sands, as reflected in the increase in basal sandy layers towards the centre of the basin (Fig. 6). These mostly fine sands (northern cores in Fig. 4) that are sourced from the gradual, relatively shore-distal slopes of the Weggis failures are likely responsible for the fine sand layer that is present towards the top of MT I in nearly all cores.

The multi-pulsed turbidites in the MT I depocentre in the south of the megaturbidite are thus likely the result of amalgamation of fine distal Weggis and Rietsort sands (Fig. 4), but they also exhibit basal medium sands. As the seismic data indicates that these sands continue below the Weggis MTDs (Fig. 3), the medium sands in this area are likely sourced from the steep southern slopes. Based on the terminology by Van Daele *et al.* (2017), the megaturbidite may thus be referred to as an 'amalgamated turbidite with a multi-pulsed character', with a more stacked or amalgamated appearance of the sandy beds, depending on the location.

Seiche influence on megaturbidite deposition (MT IIa, MT IIb and MT III)

The thin alterations of finer/coarser lamina of Unit MT IIa, revealed by CT scanning, are interpreted to have formed under influence of seiche-induced bottom currents (Figs 8 and 9). Seiche-induced bottom currents likely sorted the very fine sand and silt that was initially brought into suspension by mass movements and turbidity currents: during moments of maximum bottom-current intensity the coarser laminae are deposited, while moments of slack water allowed finer suspended grains to settle (Fig. 10). It is important to note that the seiche laminae occur only in the periphery of the depocentre (Fig. 9), where conditions were ideal for their deposition and preservation. This points towards a depth dependency for the deposition of the seiche laminae, requiring the combination of a particular hydrodynamical energy, sediment supply and water depth. During seiching, sediments at shallow water depths with vigorous seiche-generated currents are expected to be eroded. In deeper water, where seiche-generated currents are weak or non-existent, gradual deposition
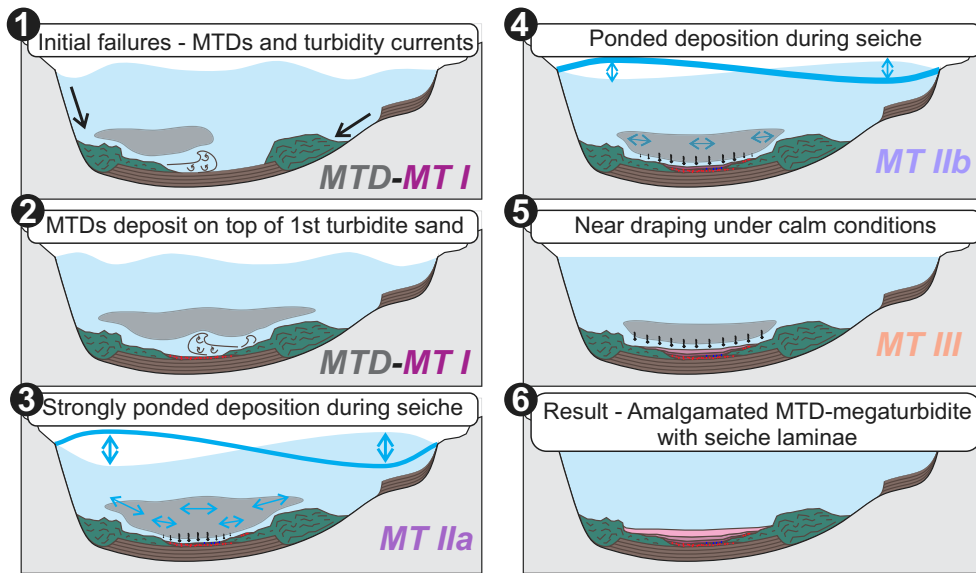
Fig. 10. Cartoon illustrating the sedimentary processes that occurred during the 1601 CE earthquake event at Lake Lucerne.

from suspended sediments can be expected, without seiche influence. Therefore, it is proposed that water depth is a crucial factor determining where and when seiches are able to influence sedimentation such that laminations are deposited and preserved. The set of seiche laminae found in Unit MT IIa supports the previously proposed hypothesis that seiche-induced currents are able to influence sedimentation (Siegenthaler *et al.*, 1987; Beck *et al.*, 2007; Campos *et al.*, 2013), although specific conditions need to be met, and the absence of evidence in one location is by no means proof for the absence of a seiche. In the Vitznau Basin megaturbidite, it seems that seiche-current sorting only influenced very fine sand (<125 μm) and finer sediments (median *ca* 7 to 10 μm), and did not rework the deposited medium sand turbidites.

In MT IIb, the grain size decreases gradually (median *ca* 5 to 7 μm; barely sand remaining) indicating that sedimentation becomes increasingly controlled by suspension fallout (Fig. 7). The seiche laminae that are still somewhat present in MT IIb are found at shallower water depths than those of MT IIa (Fig. 9). This confirms that, as the basin fills with sediment and the hydrodynamical energy decreases, the deposition and preservation of the seiche laminae moves towards shallower water depths. The diminishing influence of the lake seiche is also reflected by the declination and MAD variations that occur throughout the megaturbidite. In MT IIb, the variable declination with higher MAD values indicate that seiche currents still controlled sediment deposition, preventing the magnetic moments of the grains to fully align with the direction of the earth magnetic field and thus inducing some noise in the recording of the earth magnetic field. In contrast, the stable background declination with low MAD values (MAD <2°) in MT III illustrate a phase where grains are deposited by 'pure' suspension fallout, under calm conditions where the magnetic moments of the grains are allowed to align with the direction of the Earth magnetic field. In this final phase of megaturbidite deposition the absence of seiche currents allows the remaining suspended fine silt and clay [median *ca* 5 μm; maximum (99th percentile) *ca* 50 μm] to settle down. They cover the previous deposits in the entire deep basin, resulting in the relatively uniform distribution of MT III (Fig. 9).

In summary, the seiche seems to have an important role in shaping megaturbidites (and homogenites) into their characteristic basin-focused geometry (Siegenthaler *et al.*, 1987; Chapron *et al.*, 1999; Beck, 2009; Mulder *et al.*, 2009; Fig. 10). Following initial turbidity currents that bring large amounts of suspended sediment to the deep basin; first, relatively strong seiche currents inhibit deposition in the shallow parts of the

deep basin. The decreasing energy of the peak currents then progressively allows deposition in the shallower areas, while deposition in the depocentre continues. Finally, when all currents cease, settling of the remaining suspended silts and clays will result in a homogenous deposit over a large area, but still with some focusing in the depocentre, where most suspended material accumulated and currents cease first. In the absence of seiche currents, the authors would not expect to observe the ponded geometry of especially MT IIa and MT IIb, but rather distributions that still somehow relate to their source area, similar to the MT I distribution.

Implications for interpreting sandy layers and laminae in megaturbidites and implications for the synchronicity criterion

Determining whether layers or laminae result from tractional reworking in a single flow, pulsing within a flow, turbidite amalgamation or seiche reworking, is key to interpret the trigger of the flows that caused the deposit. Synchronous triggering ('synchronicity criterion') can be evidenced by pulsing or turbidite amalgamation and in turn be used to establish an earthquake trigger. Synchronous failure at a different location has for example been evidenced by showing variable flow directions or geochemical composition in separate pulses of a turbidite (e.g. Gutiérrez-Pastor *et al.*, 2013; Van Daele *et al.*, 2014). Without such data it remains a major challenge to prove synchronous triggering, especially from a single core, in part due to poor understanding of turbidite amalgamation/stacking processes and how oscillating seiche currents are archived in sedimentary records. The present study shows that, while interpreting the origin of layers and laminae in a single core may be difficult to impossible, transects of several cores across the megaturbidite can shed light on the development and thus origin of these layers. These core transects show – to our knowledge – for the first time stacking of MTDs on – synchronously triggered – turbidites, and such stacking is even visible on very-high-resolution reflection seismic profiles, allowing detailed mapping. It is inferred that the basal sandy layers of the turbidite likely represent multiple pulses triggered by the separate slope failures that can be identified along the lake margins. As the sandy layers are not separated by clear fine-grained, muddy beds (Wils *et al.*, 2021), these can be considered indicative for synchronous failures. In the case of the 1601

Lake Lucerne deposit, there is a clear separation in grain size between the sandy sediments directly deposited under the influence of the initial turbidity currents, and the very-fine sandy to silty muds that have been reworked/influenced by seiche current. Such grain-size break, followed by a strong grading has been shown frequently in megaturbidites (e.g. Van Daele *et al.*, 2015; Praet *et al.*, 2017; Leithold *et al.*, 2019) and has also inspired the division into a lower 'turbidite' and an upper 'homogenite' subunit of megaturbidites (Carrillo *et al.*, 2008; Çağatay *et al.*, 2012; Campos *et al.*, 2013). The presented data thus suggests that layering in the lower sandy interval is more likely a reflection of amalgamation of synchronous turbidity currents, while the laminations near the base of the muddy 'homogenite' result from seiche-induced currents. While the grain sizes that can be remobilized by a seiche will be different for each lake and even each single event (depending on the basin size, depth and landslide characteristics), it is not unrealistic to assume that the initial turbidity currents will systematically have a higher energy then the resulting seiche currents. Hence, a grain-size break will consistently indicate the change from the short-lived high-energy turbidity currents to the more prolonged, but lower energy, seiching. Finally, while these oscillating seiche currents can result in regular lamination in some locations, they do not everywhere, and the absence of these laminations is not necessarily proof for the absence of a seiche.

CONCLUSIONS

This study investigates sedimentation processes related to the 1601 CE central Switzerland earthquake in Lake Lucerne, providing the first high-detailed spatial reconstruction of megaturbidite deposition in a lake (Fig. 10). An integrated approach using multiple data sources (seismic reflection data, medical and μCT scanning, grain-size analysis and palaeomagnetic analysis) was used in order to link some of the sandy turbidite beds to their source areas and to identify the relative timing of the different turbidity currents and mass flows. The analysis shows that the base of the megaturbidite generally consists of amalgamated turbidites, which have a stacked appearance at some sites. This study further identifies the deposition of a mass-transport deposit (MTD) on top of a turbidite, as the Weggis mass flows overrode earlier deposited turbidite sands originating

from near-shore slope failures. While the sandy base of the megaturbidite was deposited rapidly by turbidity currents, its upper, fine-grained sequence was deposited more gradually and under the influence of bottom currents induced by the reported seiche in Lake Lucerne. The computed tomography (CT) data revealed a sedimentological imprint of the lake seiche, expressed as thin laminations deposited on top of the turbidite sands, but only near the periphery of depositional areas. The lake seiche thus appears to only have influenced finer sediments (very fine sand and mud) and its influence is strongly dependent on water depth. This implies that seiche laminae could easily be 'missed' in palaeoseismological reconstructions based on a single core, usually taken in the (depo)centre of a lake basin.

Overall, this study illustrates that interpretations regarding the depositional process of megaturbidites should rely on a detailed analysis of the deposit, both in terms of its spatial and internal variability. The approach that was applied here – CT scanning the megaturbidite base and tracing turbidites back to their source area – is useful for recognizing palaeo-earthquake induced deposits in other lakes. It shows that multiple sand layers ('pulses') resulting from turbidite amalgamation can be distinguished (due to synchronous triggering from different sources), and that the 1601 lake seiche resulted in an identifiable sedimentological imprint (seiche-induced laminae). Without evidence for clear variations in the mineralogical composition or flow directions of the basal sandy layers of a megaturbidite, deriving an earthquake trigger for these deposits remains delicate. Nevertheless, by benefitting from multiple transects across the megaturbidite and high-resolution bathymetric data, this study shows that the basal sandy layers of the megaturbidite most likely stem from sediment failures that occurred at different parts of the lake, fulfilling the synchronicity criterion. Together with the evidence for a lake seiche, these sedimentary characteristics thus strongly suggest earthquake triggering, as documented by historical accounts. Similar deposits found in the sedimentary record at other sites can thus likely be considered as evidence for the occurrence of past earthquakes.

ACKNOWLEDGEMENTS

DATA AVAILABILITY STATEMENT

The associated data can be found at the Bolin Center Database: https://bolin.su.se/data/vermassen-2023-lake-lucerne-1.

REFERENCES

Adams, J. (1990) Paleoseismicity of the Cascadia subduction zone: evidence from turbidites off the Oregon-Washington margin. *Tectonics*, **9**, 569–583.

Avşar, U., **Hubert-Ferrari, A.**, **De Batist, M.**, **Lepoint, G.**, **Schmidt, S.** and **Fagel, N.** (2014) Seismically-triggered organic-rich layers in recent sediments from Göllüköy Lake (north Anatolian fault, Turkey). *Quat. Sci. Rev.*, **103**, 67–80.

Baas, J.H., **Best, J.L.**, **Peakall, J.** and **Wang, M.** (2009) A phase diagram for turbulent, transitional, and laminar clay suspension flows. *J. Sediment. Res.*, **79**, 162–183.

Baas, J.H., **Best, J.L.** and **Peakall, J.** (2016) Predicting bedforms and primary current stratification in cohesive mixtures of mud and sand. *J. Geol. Soc. London*, **173**, 12–45.

Beck, C. (2009) Late quaternary lacustrine paleo-seismic archives in North-Western Alps: examples of earthquake-origin assessment of sedimentary disturbances. *Earth-Sci. Rev.*, **96**, 327–344.

Beck, C., **Mercier de Lépinay, B.**, **Schneider, J.L.**, **Cremer, M.**, **Çağatay, N.**, **Wendenbaum, E.**, **Boutareaud, S.**, **Ménot, G.**, **Schmidt, S.**, **Weber, O.**, **Eris, K.**, **Armijo, R.**, **Meyer, B.**, **Pondard, N.**, **Gutscher, M.A.**, **Turon, J.L.**, **Labeyrie, L.**, **Cortijo, E.**, **Gallet, Y.**, **Bouquerel, H.**, **Gorur, N.**, **Gervais, A.**, **Castera, M.H.**, **Londeix, L.**, **de Rességuier, A.** and **Jaouen, A.** (2007) Late quaternary co-seismic sedimentation in the sea of Marmara's deep basins. *Sediment. Geol.*, **199**, 65–89.

Bertrand, S., **Charlet, F.**, **Chapron, E.**, **Fagel, N.** and **De Batist, M.** (2008) Reconstruction of the Holocene seismotectonic activity of the southern Andes from seismites recorded in Lago Icalma, Chile, 39 S. *Palaeogeogr. Palaeoclimatol. Palaeoecol.*, **259**, 301–322.

Blott, S.J. and **Pye, K.** (2001) GRADISTAT: a grain size distribution and statistics package for the analysis of unconsolidated sediments. *Earth Surf. Process. Landforms*, **26**, 1237–1248.

Bondevik, S., **Gjevik, B.** and **Sørensen, M.B.** (2013) Norwegian seiches from the giant 2011 Tohoku earthquake. *Geophys. Res. Lett.*, **40**, 3374–3378.

Bouma, A.H. (1987) Megaturbidite: An acceptable term? *Geo-Marine Lett.*, **7**, 63–67.

Çağatay, M.N., **Erel, L.**, **Bellucci, L.G.**, **Polonia, A.**, **Gasperini, L.**, **Eriş, K.K.**, **Sancar, Ü.**, **Biltekin, D.**,

Uçarkuş, G. and **Ülgen, U.B.** (2012) Sedimentary earthquake records in the İzmit gulf, sea of Marmara, Turkey. *Sediment. Geol.*, **282**, 347–359.

Campos, C., **Beck, C.**, **Crouzet, C.**, **Carrillo, E.**, **Van Welden, A.** and **Tripsanas, E.** (2013) Late quaternary paleoseismic sedimentary archive from deep central gulf of Corinth: time distribution of inferred earthquake-induced layers. *Ann. Geophys.*, **56**, 1–15.

Carrillo, E., **Beck, C.**, **Audemard, F.A.**, **Moreno, E.** and **Ollarves, R.** (2008) Disentangling late quaternary climatic and seismo-tectonic controls on Lake Mucubají sedimentation (Mérida Andes, Venezuela). *Palaeogeogr. Palaeoclimatol. Palaeoecol.*, **259**, 284–300.

Chapron, E., **Beck, C.**, **Pourchet, M.** and **Deconinck, J.F.** (1999) 1822 earthquake-triggered homogenite in Lake Le Bourget (NW Alps). *Terra Nov.*, **11**, 86–92.

Cita, M.B., **Camerlenghi, A.** and **Rimoldi, B.** (1996) Deep-sea tsunami deposits in the eastern Mediterranean: new evidence and depositional models. *Sediment. Geol.*, **104**, 155–173.

Cnudde, V. and **Boone, M.N.** (2013) High-resolution X-ray computed tomography in geosciences: a review of the current technology and applications. *Earth-Sci. Rev.*, **123**, 1–17.

Cysat, R. (1601) Collectanea Chronica und denkwu rdige Sachen pro Chronica Lucernensi et Helvetiae. In: *Quellen und Forschungen zur Kulturgeschichte von Luzern und der Innerschweiz* (Ed. Schmid, J.), pp. 882–888. Luzern: Stadt Luzern.

Fanetti, D., **Anselmetti, F.S.**, **Chapron, E.**, **Sturm, M.** and **Vezzoli, L.** (2008) Megaturbidite deposits in the Holocene basin fill of Lake Como (southern Alps, Italy). *Palaeogeogr. Palaeoclimatol. Palaeoecol.*, **259**, 323–340.

Girardclos, S., **Schmidt, O.T.**, **Sturm, M.**, **Ariztegui, D.**, **Pugin, A.** and **Anselmetti, F.S.** (2007) The 1996 AD delta collapse and large turbidite in Lake Brienz. *Mar. Geol.*, **241**, 137–154.

Goldfinger, C. (2009) Sub-aqueous paleoseismology. In: *Paleoseismology* (Ed. McCalpin, J.P.), *International Geophysics*, **95**, 119–170. Cambridge, MA: Academic Press.

Gisler, M., **Fäh, D.** and **Kästli, P.** (2004) Historical seismicity in Central Switzerland. *Eclogae Geologicae Helvetiae*, **97** (2), 221–236.

Granin, N.G., **Radziminovich, N.A.**, **De Batist, M.**, **Makarov, M.M.**, **Chechelnitcky, V.V.**, **Blinov, V.V.**, **Aslamov, I.A.**, **Gnatovsky, R.Y.**, **Poort, J.** and **Psakhie, S.G.** (2018) Lake Baikal's response to remote earthquakes: lake-level fluctuations and near-bottom water layer temperature change. *Mar. Pet. Geol.*, **89**, 604–614.

Gutiérrez-Pastor, J., **Nelson, C.H.**, **Goldfinger, C.** and **Escutia, C.** (2013) Sedimentology of seismo-turbidites off the Cascadia and northern California active tectonic continental margins, Northwest Pacific Ocean. *Mar. Geol.*, **336**, 99–119.

Hilbe, M. and **Anselmetti, F.S.** (2014) Signatures of slope failures and river-delta collapses in a perialpine lake (Lake Lucerne, Switzerland). *Sedimentology*, **61**, 1883–1907.

Hilbe, M. and **Anselmetti, F.S.** (2015) Mass movement-induced tsunami Hazard on Perialpine Lake Lucerne (Switzerland): scenarios and numerical experiments. *Pure Appl. Geophys.*, **172**, 545–568.

Hilbe, M., **Anselmetti, F.S.**, **Eilertsen, R.**, **Hansen, L.** and **Wildi, W.** (2011) Subaqueous morphology of Lake Lucerne (Central Switzerland): implications for mass movements and glacial history. *Swiss J. Geosci.*, **104**, 425–443.

Hounsfield, G.N. (1973) Computerized transverse axial scanning (tomography): Part 1. Description of system. *The British journal of radiology* **46**, 552.

Kastens, K.A. (1984) Earthquakes as a triggering mechanism for debris flows and turbidites on the Calabrian ridge. *Mar. Geol.*, **55**, 13–33.

Kastens, K.A. and **Cita, M.B.** (1981) Tsunami-induced sediment transport in the abyssal Mediterranean-Sea. *Geol. Soc. Am. Bull.*, **92**, 845–857.

Kirschvink, J.L. (1980) The least-squares line and plane and the analysis of palaeomagnetic data. *Geophys. J. Roy. Astron. Soc.*, **62**, 699–718.

Kvale, A. (1955) Seismic seiches in Norway and England during the Assam earthquake of august 15, 1950. *Bull. Seismol. Soc. Am.*, **45**, 93–113.

Leithold, E.L., **Wegmann, K.W.**, **Bohnenstiehl, D.R.**, **Joyner, C.N.** and **Pollen, A.F.** (2019) Repeated megaturbidite deposition in Lake crescent, Washington, USA, triggered by Holocene ruptures of the Lake Creek-Boundary Creek fault system. *Bull. Geol. Soc. Am.*, **131**, 2039–2055.

L'Heureux, J.-S., **Longva, O.**, **Hansen, L.** and **Vanneste, M.** (2014). In: *The 1930 Landslide in Orkdalsfjorden: Morphology and Failure Mechanism BT - Submarine Mass Movements and Their Consequences: 6th International Symposium* (Eds Krastel, S., Behrmann, J.-H., Völker, D., Stipp, M., Berndt, C., Urgeles, R., Chaytor, J., Huhn, K., Strasser, M. and Harbitz, C.B.), pp. 239–247. Springer International Publishing, Cham.

Louis, K., **Bänninger, P.**, **Luterbacher, J.** and **Zwyer, T.** (2008) Der Schuttstrom vom 15./16. Juli 1795 in Weggis - Rekonstruktion des Ereignisses und Beurteilung des Vorhandenen Gefahrenpotenzials. *Bull. fuer Angew. Geol.*, **13**, 55–81.

Masschaele, B., **Dierick, M.**, **Van Loo, D.**, **Boone, M.N.**, **Brabant, L.**, **Pauwels, E.**, **Cnudde, V.** and **Van Hoorebeke, L.** (2013) HECTOR: a 240kV micro-CT setup optimized for research. *J. Phys.*, **463**, 12012.

McCulloch, D.S. (1966) Slide-induced waves, seiching and ground fracturing caused by the earthquake of March 27, 1964 at Kenai Lake, Alaska. 41 pp.

Moernaut, J. and **De Batist, M.** (2011) Frontal emplacement and mobility of sublacustrine landslides: results from morphometric and seismostratigraphic analysis. *Mar. Geol.*, **285**, 29–45.

Mulder, T., **Zaragosi, S.**, **Razin, P.**, **Grelaud, C.**, **Lanfumey, V.** and **Bavoil, F.** (2009) A new conceptual model for the deposition process of homogenite: application to a cretaceous megaturbidite of the western Pyrenees (Basque region, SW France). *Sediment. Geol.*, **222**, 263–273.

Nakajima, T. and **Kanai, Y.** (2000) Sedimentary features of seismoturbidites triggered by the 1983 and older historical earthquakes in the eastern margin of the Japan Sea. *Sediment. Geol.*, **135**, 1–19.

Nelson, C.H., **Gutiérrez Pastor, J.**, **Goldfinger, C.** and **Escutia, C.** (2012) Great earthquakes along the Western United States continental margin: implications for hazards, stratigraphy and turbidite lithology. *Nat. Hazards Earth Syst. Sci.*, **12**, 3191–3208.

Nigg, V., **Bacigaluppi, P.**, **Vetsch, D.F.**, **Vogel, H.**, **Kremer, K.** and **Anselmetti, F.S.** (2021) Shallow-water tsunami deposits: evidence from sediment cores and numerical wave propagation of the 1601 CE Lake Lucerne event. *Geochem. Geophys. Geosyst.*, **22**, e2021GC009753.

Polonia, A., **Bonatti, E.**, **Camerlenghi, A.**, **Lucchi, R.G.**, **Panieri, G.** and **Gasperini, L.** (2013) Mediterranean

megaturbidite triggered by the AD 365 Crete earthquake and tsunami. *Sci. Rep.*, **3**, 1–12.

Postma, G., Nemec, W. and Kleinspehn, K.L. (1988) Large floating clasts in turbidites: a mechanism for their emplacement. *Sediment. Geol.*, **58**, 47–61.

Praet, N., Moernaut, J., Van Daele, M., Boes, E., Haeussler, P.J., Strupler, M., Schmidt, S., Loso, M.G. and De Batist, M. (2017) Paleoseismic potential of sublacustrine landslide records in a high-seismicity setting (south-Central Alaska). *Mar. Geol.*, **384**, 103–119.

Praet, N., Van Daele, M., Moernaut, J., Mestdagh, T., Vandorpe, T., Jensen, B.J.L., Witter, R.C., Haeussler, P.J. and De Batist, M. (2022) Unravelling a 2300 year long sedimentary record of megathrust and intraslab earthquakes in proglacial Skilak Lake, south-Central Alaska. *Sedimentology*, **69**, 2151–2180.

Reeder, M.S., Rothwell, R.G. and Stow, D.A.V. (2000) Influence of sea level and basin physiography on emplacement of the late Pleistocene Herodotus Basin Megaturbidite, SE Mediterranean Sea. *Mar. Pet. Geol.*, **17**, 199–218.

Schneider, C.A., Rasband, W.S. and Eliceiri, K.W. (2012) NIH image to ImageJ: 25 years of image analysis. *Nat. Methods*, **9**, 671–675.

Schnellmann, M. P. (2004). Late quaternary mass-movements in a perialpine lake (Lake Lucerne, Switzerland). Sedimentary processes, natural hazards and paleoseismic reconstructions. PhD thesis, ETH Zürich, 131 pp.

Schnellmann, M., Anselmetti, F.S., Giardini, D. and McKenzie, J.A. (2005) Mass movement-induced fold-and-thrust belt structures in unconsolidated sediments in Lake Lucerne (Switzerland). *Sedimentology*, **52**, 271–289.

Schnellmann, M., Anselmetti, F.S., Giardini, D., McKenzie, J.A. and Ward, S.N. (2002) Prehistoric earthquake history revealed by lacustrine slump deposits. *Geology*, **30**, 1131–1134.

Schnellmann, M., Anselmetti, F.S., Giardini, D. and McKenzie, J.A. (2006) 15,000 years of mass-movement history in Lake Lucerne: implications for seismic and tsunami hazards. *Eclogae Geol. Helv.*, **99**, 409–428.

Schwarz-Zanetti, G., Deichmann, N., Fäh, D., Giardini, D., Jimenez, M.J., Masciadri, V., Schibler, R. and Schnellmann, M. (2003) The earthquake in Unterwalden on September 18, 1601: a historico-critical macroseismic evaluation. *Eclogae Geol. Helv.*, **96**, 441–450.

Siegenthaler, C., Finger, W., Kelts, K. and Wang, S. (1987) Earthquake and Seiche deposits in Lake Lucerne, Switzerland. *Eclogae Geol. Helv.*, **80**, 241–260.

Stevenson, C.J., Peakall, J., Hodgson, D.M., Bell, D. and Privat, A. (2020) TB or not TB: banding in turbidite sandstones. *J. Sediment. Res.*, **90**, 821–842.

Van Daele, M., Cnudde, V., Duyck, P., Pino, M., Urrutia, R. and De Batist, M. (2014) Multidirectional, synchronously-triggered seismo-turbidites and debrites revealed by X-ray computed tomography (CT). *Sedimentology*, **61**, 861–880.

Van Daele, M., Moernaut, J., Doom, L., Boes, E., Fontijn, K., Heirman, K., Vandoorne, W., Hebbeln, D., Pino, M., Urrutia, R., Brümmer, R. and De Batist, M. (2015) A comparison of the sedimentary records of the 1960 and 2010 great Chilean earthquakes in 17 lakes: implications for quantitative lacustrine palaeoseismology. *Sedimentology*, **62**, 1466–1496.

Van Daele, M., Meyer, I., Moernaut, J., De Decker, S., Verschuren, D. and De Batist, M. (2017) A revised classification and terminology for stacked and amalgamated turbidites in environments dominated by (hemi)pelagic sedimentation. *Sediment. Geol.*, **357**, 72–82.

Vlassenbroeck, J., Masschaele, B.C., Dierick, M., Cnudde, V., De Witte, Y., Pieters, K., Van Hoorebeke, L. and Jacobs, P. (2007) Recent developments in the field of X-ray Nano- and Micro-CT at the Centre for X-ray tomography of the Ghent University. *Microsc. Microanal.*, **13**, 184–185.

Weeks, R., Laj, C., Endignoux, L., Fuller, M., Roberts, A., Manganne, R., Blanchard, E. and Goree, W. (1993) Improvements in long-core measurement techniques: applications in palaeomagnetism and palaeoceanography. *Geophys. J. Int.*, **114**, 651–662.

Wils, K., Deprez, M., Kissel, C., Vervoort, M., Van Daele, M., Daryono, M.R., Cnudde, V., Natawidjaja, D.H. and De Batist, M. (2021) Earthquake doublet revealed by multiple pulses in lacustrine seismo-turbidites. *Geology*, **49**, 1301–1306.

Withers, P.J., Bouman, C., Carmignato, S., Cnudde, V., Grimaldi, D., Hagen, C.K., Maire, E., Manley, M., Du Plessis, A. and Stock, S.R. (2021) X-ray computed tomography. *Nat. Rev. Methods Prim.*, **1**, 1–21.

Zuffa, G.G., Normark, W.R., Serra, F. and Brunner, C.A. (2000) Turbidite megabeds in an oceanic Rift Valley recording jokulhlaups of late Pleistocene glacial lakes of the western United States. *J. Geol.*, **108**, 253–274.

Supporting Information

Additional information may be found in the online version of this article:

Figure S1. (A) Seismic profile with indications of core sites. (B) Core photographs of cores along the transect, with CT scan of the top section of core LU14-11, illustrating the rockslide deposit induced by the rockfall that occurred in the quarry at Obermatt in 1964.